Opto-Electronic Science

Review

2022, Vol. 1, No. 6

DOI: 10.29026/oes.2022.220005

Femtosecond laser-induced periodic structures: mechanisms, techniques, and applications

Yuchan Zhang[1†], Qilin Jiang[1†], Mingquan Long[1], Ruozhong Han[1], Kaiqiang Cao[1*], Shian Zhang[1], Donghai Feng[1], Tianqing Jia[1,2*], Zhenrong Sun[1], Jianrong Qiu[3] and Hongxing Xu[1]

Over the past two decades, femtosecond laser-induced periodic structures (femtosecond-LIPSs) have become ubiquitous in a variety of materials, including metals, semiconductors, dielectrics, and polymers. Femtosecond-LIPSs have become a useful laser processing method, with broad prospects in adjusting material properties such as structural color, data storage, light absorption, and luminescence. This review discusses the formation mechanism of LIPSs, specifically the LIPS formation processes based on the pump-probe imaging method. The pulse shaping of a femtosecond laser in terms of the time/frequency, polarization, and spatial distribution is an efficient method for fabricating high-quality LIPSs. Various LIPS applications are also briefly introduced. The last part of this paper discusses the LIPS formation mechanism, as well as the high-efficiency and high-quality processing of LIPSs using shaped ultrafast lasers and their applications.

Keywords: laser-induced periodic structures (LIPSs); formation mechanisms; femtosecond pulse shaping; pump-probe imaging; structural color; birefringent effects; optical absorption; photoluminescence

Zhang YC, Jiang QL, Long MQ, Han RZ, Cao KQ et al. Femtosecond laser-induced periodic structures: mechanisms, techniques, and applications. *Opto-Electron Sci* **1**, 220005 (2022).

Introduction

Femtosecond lasers have ultrashort pulse durations and high peak powers[1]. The interaction between femtosecond laser and matter has the advantages of minimal thermal effect and no material selectivity[2,3]. Compared with nanosecond and other long-pulse lasers, femtosecond lasers could induce more regular and deeper periodic structures on different types of materials, such as metals, semiconductors, dielectrics, and polymers, without being overwhelmed by huge thermal effects[4–14].

Laser-induced periodic structures (LIPSs) have been intensively studied since 1965 when Birnbaum et al. found LIPSs on the surface of germanium and gallium arsenide[15,16]. Over the past two decades, ultrafast laser technology has developed rapidly. Femtosecond LIPSs (femtosecond-LIPSs) have become ubiquitous in a variety of materials, including metals, semiconductors, dielectrics, and polymers[4–9,17–31]. The periods of LIPSs change significantly with the laser fluence and the number of overlapping pulses. Based on the ratio of the period

[1]State Key Laboratory of Precision Spectroscopy, School of Physics and Materials Science, East China Normal University, Shanghai 200062, China; [2]Collaborative Innovation Center of Extreme Optics, Shanxi University, Taiyuan 030006, China; [3]State Key Laboratory of Optical Instrumentation, Zhejiang University, Hangzhou 310027, China.

[†]These authors contributed equally to this work.

*Correspondence: KQ Cao, E-mail: kqcao@lps.ecnu.edu.cn; TQ Jia, E-mail: tqjia@phy.ecnu.edu.cn

Received: 22 March 2022; Accepted: 10 May 2022; Published online: 21 June 2022

(Λ) to the laser wavelength (λ), LIPSs are divided into low-spatial-frequency LIPSs (LSFLs, $\Lambda > 0.5\lambda$) and high-spatial-frequency LIPSs (HSFLs, $\Lambda < 0.5\lambda$)[4], as shown in Fig. 1. However, the formation mechanism of femtosecond-LIPSs does not yet have a clear explanation.

Femtosecond-LIPSs have become a useful laser processing method, with broad prospects for adjusting material properties[9,32–38] . HSFLs on the surfaces and interiors of dielectrics demonstrate birefringence effects, which have been used in data storage and waveplates[34,36,38]. LIPSs produce a significant dispersion of incident light and have been used to prepare pure and bright structural color surface[32,35]. Composite structures with LIPSs can enhance light absorption and luminescence and adjust the wetting properties of a material surface[33,37,39]. The anisotropic electrical properties of LIPSs are an emerging research topic[40,41].

The main contents of this review are as follows. Section *Several models of LIPS formation* discusses the formation mechanism of LIPSs. Section *Ultrafast dynamics of LIPS formation based on pump-probe imaging* presents the ultrafast dynamics studied by the pump-probe imaging method. The pulse shaping of a femtosecond laser in the temporal –frequency domain, polarization, and spatial distribution is an efficient method for fabricating regular LIPSs with high efficiency, as described in Section *Efficient fabrication of high-quality LIPSs with shaped ultrafast laser pulses*. Section *Femtosecond laser direct writing of <100 nm nanostructures* introduces promising methods for laser processing nanostructures with feature sizes smaller than 100 nm. In the Section *Applications of LIPSs*, we briefly introduce LIPS applications in the fields of data storage, structural color surfaces, light absorption and luminescence enhancement, and the adjustment of conductive properties. The last section presents the outlook on the LIPSs. storage, structural color surfaces, light absorption and luminescence enhancement, and the adjustment of conductive properties. The last section presents the outlook on the LIPSs.

Several models of LIPS formation

The formation of periodic nanostructures after irradiation with a single laser beam is an interesting phenomenon. In particular, the periods of femtosecond-LIPSs change significantly with the laser fluence and the number of overlapping pulses, which renders the formation mechanism of LIPSs more complicated to determine. Numerous experimental, theoretical, and numerical studies have been performed, and several models have been proposed to explain the formation of LIPSs[9,16–18,20,21,25,42], which are described below.

Scattering light model

After irradiation with continuous and long-pulse lasers, LSFLs perpendicular or parallel to the polarization direction formed on the surfaces of semiconductor materials, where the periods were nearly equal to the laser wavelength, λ. It was proposed that these LSFLs were caused by the interference between the incident light and scattered light from the ablated surface[16,18,43], as shown in Fig. 2. When the laser was perpendicular to the sample, period Λ was equal to laser wavelength λ. When the laser was obliquely incident at an angle θ, period $\Lambda = \lambda/ (1 \pm \sin\theta)$, where + and – represent the forward and backward scattered light, respectively[44]. This model was refined and developed by Sipe et al. They performed detailed theoretical studies and found that the generation of periodic structures depended significantly on the

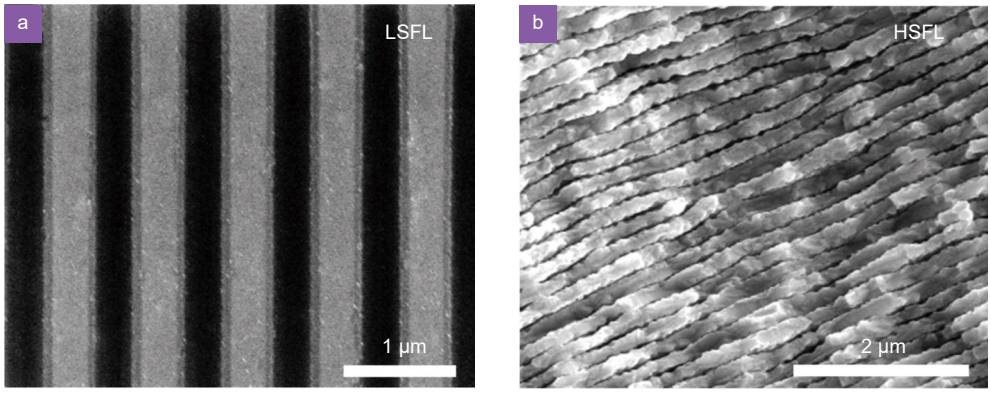

Fig. 1 | Scanning electron microscopy (SEM) images of (**a**) LSFLs on silicon[8], and (**b**) HSFLs on ZnSe induced by 800 nm femtosecond laser. Figure reproduced with permission from: (a) ref.[8], Optica Publishing Group, under the Optica Open Access Publishing Agreement; (b) ref.[9], American Physical Society.

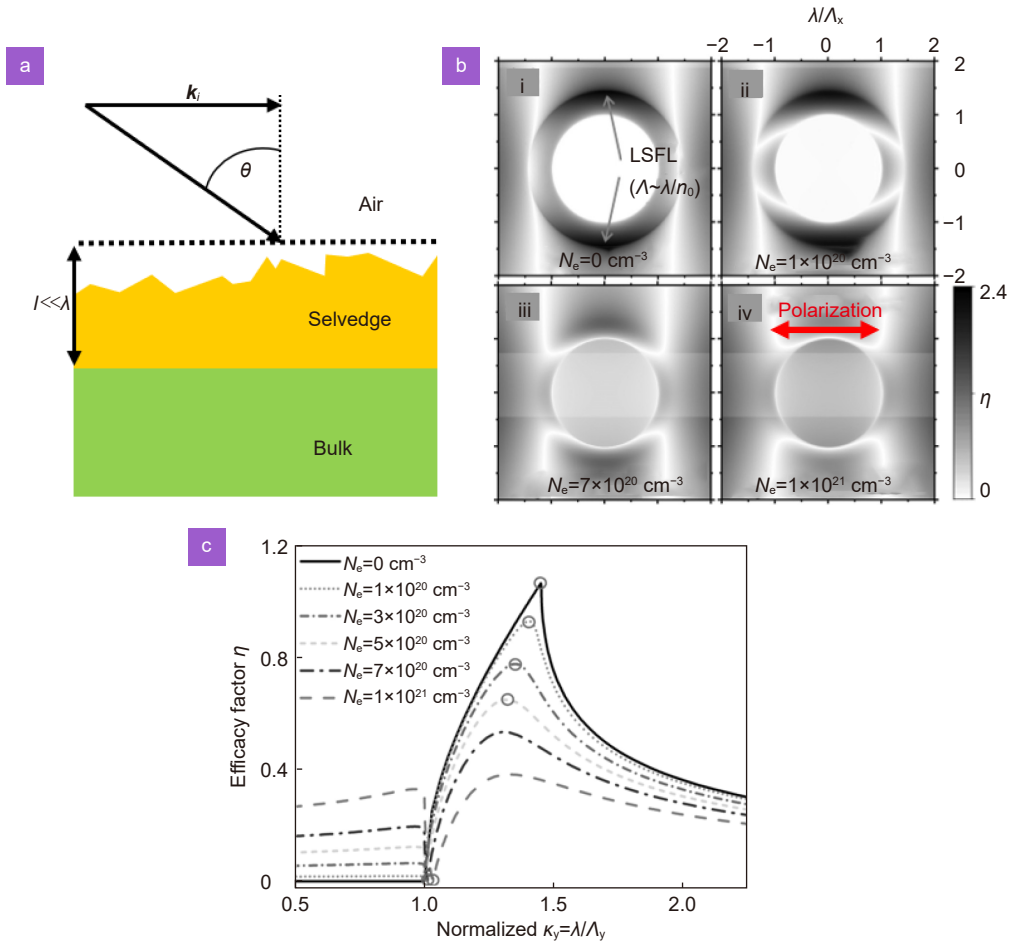

Fig. 2 | (**a**) The schematic of light irradiated on a rough surface at an incident angle θ, where $\boldsymbol{k}_i$ is the wave-vector component parallel to the surface, and l is the thickness of selvedge region. (**b**) The efficacy factor η as a function of the normalized LIPS wave vector for silica at different excited state. (**c**) The efficacy factor η along the positive k_y-axis for silica at different excitation levels, with circles marking k_y-positions where LIPS formation could be expected. Figure reproduced with permission from: (a) ref.[16], American Physical Society; (b, c) ref.[22], AIP Publishing.

roughness of the material surface[16]. Rough structures with a height significantly smaller than the laser wavelength resulted in a periodic distribution of the laser field itself. The incident angle and polarization direction highly influenced the period and orientation of the LSFLs. This model has often been used to explain classical LSFLs induced by nanosecond or continuous wave (CW) lasers.

Over the last two decades, scattering models have been developed and improved to explain the formation of femtosecond-LIPSs[45,46]. According to the Drude model, the dielectric constants of semiconductors and dielectrics depend on the numerical density of free electrons excited by femtosecond laser. According to the Sipe model, the periodic deposition of laser energy depends on the surface roughness and dielectric constants. The formation of femtosecond-LIPSs on semiconductors and dielectrics was studied by comprehensively considering the Sipe and Drude models[22,23,47,48], and developed into the Sipe-Drude model[22]. The numerical density of free electrons and dielectric constants varied with the laser fluence, wavelength, and pulse number, which further tuned the periods of LIPSs, as shown in Fig. 2.

Surface plasmon polariton model

Under femtosecond laser irradiation, a large number of free electrons are excited, forming a plasma layer on the surface of a material. The femtosecond laser further causes the collective oscillation of the surface plasma and forms surface plasmon polaritons (SPPs), as shown in Fig. 3(a). The excitation of SPPs causes a periodic distribution of the laser field and energy deposition in the free electrons. The lattice is heated, melted, or even ablated via electron–phonon coupling, which further induces the formation of LIPSs[8,21,25,48,50–62]. However, in the case of vertical incidence (Fig. 3(b)), the wave vector of the SPPs is always larger than that of the incidence light. Therefore, grating structures[42] or a single nanogroove[25,52] are

fabricated on the sample surface in advance, and the scattered light can provide an additional wave vector, $\Delta\boldsymbol{k}$, which satisfies the vector matching condition and induces SPP excitation, as shown in Fig. 3(c)[21].

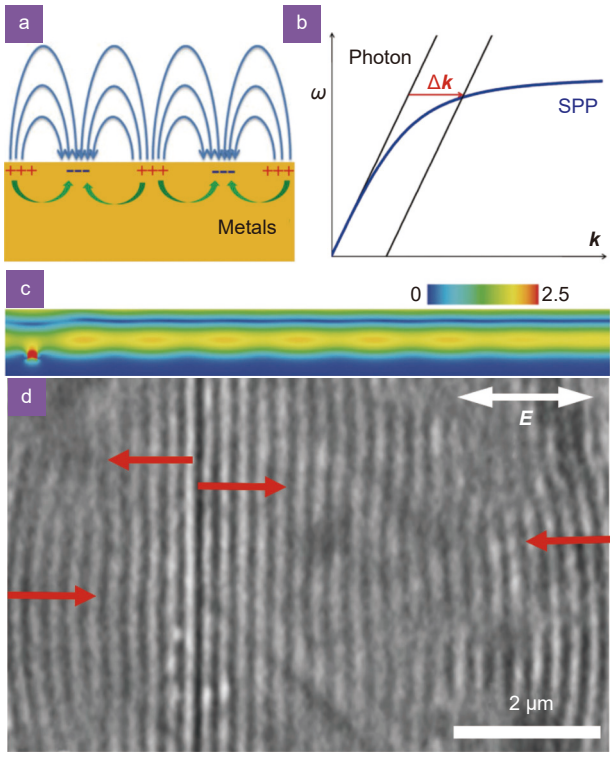

Fig. 3 | (**a**) Schematic illustration of SPPs. (**b**) Dispersion curves of SPPs and light in air. (**c**) SPP excitation on ZnO surface in the excited state launched by a groove. (**d**) The SEM image of the nanostructures on the ZnO surface irradiated by 800 nm femtosecond laser, where the LSFLs originated from the nanogroove or the ablation edge, as shown as the red arrows. Figure reproduced with permission from: (b) ref.[49], AIP Publishing; (c, d) ref.[21], American Chemical Society.

The SPP model was used to explain the formation of LSFLs on semiconductors. The periods are expressed as follows[21]

$$\Lambda = \frac{\lambda}{\frac{\lambda}{\lambda_{\rm SPP}} \pm \sin(\theta)},$$
$$\lambda_{\rm SPP} = \lambda \times {\rm Re}\left(\sqrt{\frac{\varepsilon+\varepsilon_{\rm d}}{\varepsilon\varepsilon_{\rm d}}}\right), \quad (1)$$

where $\lambda_{\rm SPP}$ is the SPP wavelength, θ is the angle of incidence, ε is the dielectric constant of the metal, and $\varepsilon_{\rm d}$ is the dielectric constant of the dielectric. Under femtosecond laser irradiation, a large number of free electrons are excited, resulting in a significant change in the dielectric constant, according to the Drude model. The SPP wavelength and LSFL period can be calculated based on the dielectric constant in the excited state, which agrees well with the experimental results for semiconductors[42,51,52]. The LSFL periods induced by femtosecond laser pulses on semiconductors and metals are always smaller than the SPP wavelengths. With more laser pulse irradiation, the LSFL-assisted SPP is coupled with the laser field, forming a positive feedback effect, and leading to the formation of shorter-period LSFLs[21].

Model of nanoplasmonic enhancement of laser field

The groove widths of HSFLs induced by femtosecond laser pulses are usually smaller than 100 nm, whereas the depth can reach hundreds of nanometers to micrometers. The widths of these periodically arranged nanogrooves are significantly smaller than the diffraction limit of the laser[17,20,63–72]. Figure 4(a) shows 20 nm-thick nanosheet-like nanostructures with a period of ~$\lambda/2n$ in fused silica (refractive index n) induced by linearly polarized 800 nm femtosecond laser pulses. It was proposed that these nanosheets were produced by the asymmetrically localized laser-field enhancement of the nanoplasma[20], as shown in Fig. 4(b).

The periodic distribution of the nanoplanes evolved from a random distribution of nanoplasma over many shots owing to the memory mechanism and mode selection. The period, $\lambda_0/2n$, is the minimum spacing required in planar metal waveguides to support this mode with the field maxima at the metal–dielectric interface[20].

Another mechanism that has been proposed for the formation of HSFLs in fused silica is photon–plasmon scattering[17]. By adjusting the pulse energy and cumulative pulse number of the 800 nm femtosecond laser, the HSFLs period varied from 140 to 320 nm. This phenomenon was interpreted in terms of the interference between the incident light field and the electric field of the bulk plasma wave, resulting in the periodic modulation of the electron concentration and structural changes in the fused silica[17].

Other models

In recent years, several other models have been proposed to explain the formation of LIPSs, such as self-organization[24,26,73], evanescent waves[74], and Coulomb explosions[75,76]. During the femtosecond laser irradiation of SiC, ZnSe, and ZnO crystals, the generation of second harmonics induces the formation of HSFLs[9,77,78]. The ripples of LSFLs on metal surfaces gradually split and evolve into HSFLs with an increase in femtosecond laser pulse irradiation[79,80].

During the femtosecond laser irradiation of semiconductor materials such as Si and ZnS, the surface plasmon layer supports two types of SPPs: those at the plasma–air interface and those at the plasma–substrate interface[81]. The local laser fluence and accumulated pulse number are key factors affecting the formation of LSFLs and HSFLs. Two SPP waves interfere with each other to form standing waves that induce the formation of HSFLs[82,83]. A femtosecond laser was obliquely incident on a stainless steel surface and induced two periodic structures, LSFLs and HSFLs, which were caused by forward- and backward-propagating SPPs, respectively[84]. Numerical simulation results using the finite-difference time-domain (FDTD) method indicated that the coherent superposition of the scattering far-field (propagation) of the microstructured surface and refracted fields induced LSFLs, while the scattering near-field (evanescent) and refracted fields induced HSFLs[85].

Ultrafast dynamics of LIPS formation based on pump-probe imaging

The phenomena of femtosecond-LIPSs are very rich, and the formation mechanisms are very complicated. Are LIPSs caused by the periodic deposition of laser energy or by self-organization during laser excitation, melting, and solidification? The propagating SPP model has been widely accepted to explain the formation of LSFLs on semiconductor and metal surfaces, however several key issues remain to be addressed. First, the SPPs on the surfaces of gold and silver are very strong[86], however it is difficult to form regular LSFLs on these noble metals[10]. Second, the periods of the LIPSs on metal surfaces are significantly smaller than the SPP wavelengths[49,87]. The further development of new methods is required to solve these problems.

Scanning electron microscopy (SEM) and atomic force microscopy (AFM) are typically used to observe LIPSs. The resolutions of these methods are very high, however they cannot be used to study the dynamics of LIPS formation. Pump-probe spectroscopy is an effective method to study the kinetics of femtosecond laser ablation[88]. However, transient images of LIPSs cannot be observed directly[19,79]. Therefore, we developed a collinear pump-probe imaging method to study the transient processes of LIPS formation[25,49,52,55,56,89]. The spatial resolution is 300 nm and the temporal resolution is 0.6 ps. To show clearly the changes in the surface microstructure, the same spot was observed at three different times: before the arrival of the pump pulse, at the designed delay time, and after the ablation spot solidified.

Figure 5 shows the optical microscope (OM) images of the transient LSFLs on the Si surface at different delay times[52]. The LSFL period was 680 ± 15 nm, and the direction was parallel to the nanogroove. The annular structures were caused by the diffraction effect of the concave lens. Surprisingly, periodic ripples quickly emerged. The transient ripples were clear at a delay time of 4.0 ps, which indicated that these ripples were due to surface melting, excluding other thermodynamics such as ablation and hydrodynamics. The AFM measurements further showed that the height fluctuation in the LSFL region was less than 0.6 nm, and had no spatial periodicity. The LSFL period was predicted based on the SPP model, and it coincided with the experimental results. The formation of LSFLs on silicon was due to the periodic energy deposition caused by the SPP excitation, rather than

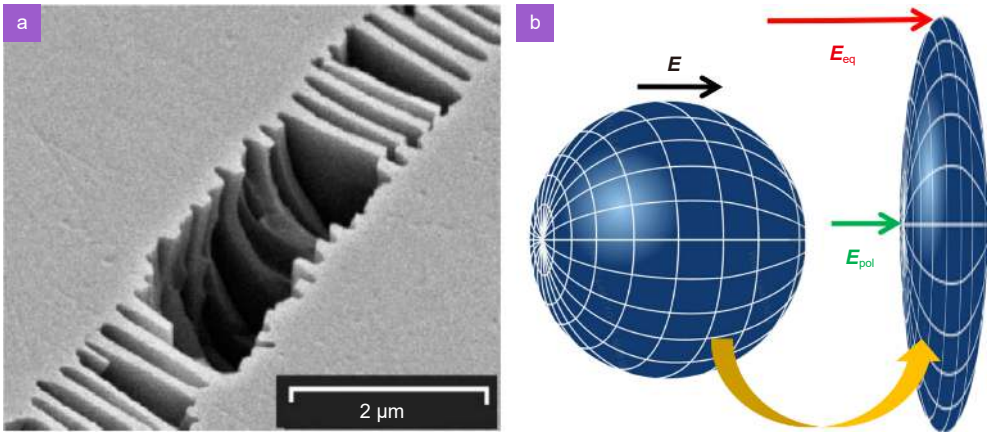

Fig. 4 | (**a**) SEM image of HSFLs inside fused silica induced by 800 nm femtosecond laser pulses. (**b**) Nanoplasma growth into plane governed by local field distribution, where $\boldsymbol{E}_{pol}$ and $\boldsymbol{E}_{eq}$ are the local fields on the polar axis and in the equatorial plane, respectively[4,20]. Figure reproduced with permission from: (a) ref.[20], American Physical Society.

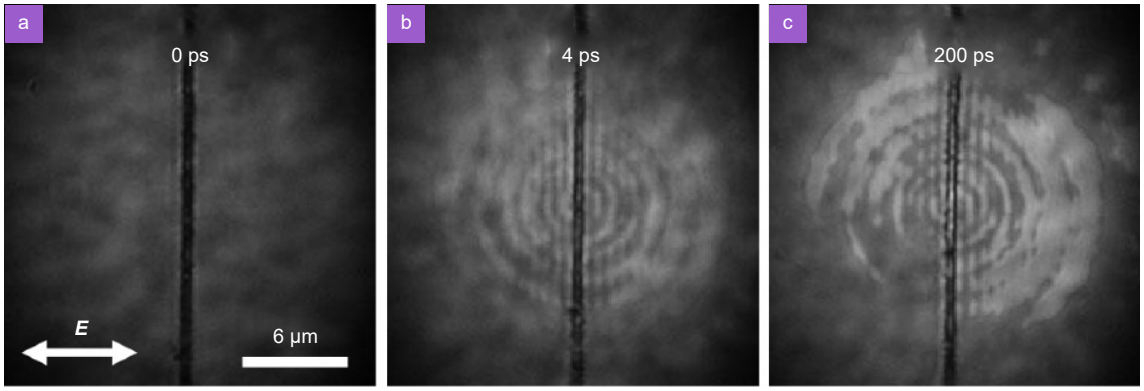

Fig. 5 | OM images of silicon surface irradiated by a single 800 nm femtosecond pulse of 0.18 J/cm². The double arrows in (**a**) show the laser polarization direction. Figure reproduced with permission from ref.[52], Optica Publishing Group, under the Optica Open Access Publishing Agreement.

self-organization processes.

The pump-probe imaging experiments were further carried out to investigate the role of SPPs and thermal effects on the formation of LIPSs on noble-metal surfaces[49]. Under the irradiation of the second femtosecond laser pulse, transient periodic ripples were clearly observed on the gold film, but no obvious ripples remained after the surface solidified. The surface defects produced by the first laser pulse launched SPPs on the Au film, which caused further modulated energy deposition and induced transient LIPSs. However, because of the small electron–phonon coupling coefficient of Au, the slow heat process and strong melting effect caused the ripples to disappear. When the Au film was immersed in water, the LIPSs were retained because of the high cooling rate of the molten layers[49]. These experimental results indicated that the SPPs played an important role in the formation of LIPSs, while the thermal effect greatly influenced whether the transient ripples were retained after the molten surface solidified[49] .

However, the period dependence of the LSFLs on metal surfaces was much different from the SPP model[87,90,91]. The SPP wavelengths were calculated by using the dielectric constants of silver, gold, copper, and aluminum in the ground states, which were significantly larger than the periods of LSFL ripples[10,49,92]. The d-band electrons in gold and silver could be excited to states above the Fermi surface[93,94]. The free-electron density and plasma frequency both increased with laser fluence, resulting in longer SPP wavelengths. The LSFL periods were very different from those of the SPP model, which is a difficult problem to solve.

LSFLs are typically induced by multiple laser pulses. The material at the laser focus is partially ablated after each laser pulse irradiation, which makes the formation mechanisms more difficult to understand because of the effects of the scattered light and grating coupling feedback. Therefore, theoretical and experimental studies on the LSFLs induced by a single femtosecond laser pulse provide fundamental information on the origin of LSFLs on metal surfaces[52,95–97].

Figure 6 shows the evolution of the LSFLs formed on an Au film. The transient LSFLs began to appear at 45 ± 10 ps, and become more numerous and clearer over time[25]. Between 400 and 600 ps, the ripples appear to be the most distinct and regular. The ripples are perpendicular to the laser polarization with a period of 740 ± 10 nm.

Figure 7 shows that the LSFL period increased from 685 nm to 770 nm when the fluence increased from 0.73 to 3.42 J/cm² [25], which was similar to the results for Si, GaP, and ZnO crystals[51,52,98,99]. The SPP wavelength of gold was 780 nm for 800 nm light, which was significantly larger than the experimental value. With increasing laser fluence, free-electron density became larger, which led to longer SPP wavelength and LSFL period. Obviously, there is a great deviation between the SPP theory and the experimental results.

The dielectric constant is a key factor affecting the SPP wavelength[21,25]. The dielectric constant in the ground state was usually used to study SPP on metal surfaces, which was an important factor that caused the deviation between the SPP theory and the experimental results. Therefore, Cheng et al. proposed and studied in detail the effects of hot electron localization and d-band transitions on the dielectric constant and SPP wavelength for gold at the highly excited states during femtosecond laser irradiation[25]. The LSFL period calculated by the developed SPP model decreased from 780 nm to 685 nm as the fluence increased to 0.75 J/cm². However, as F was

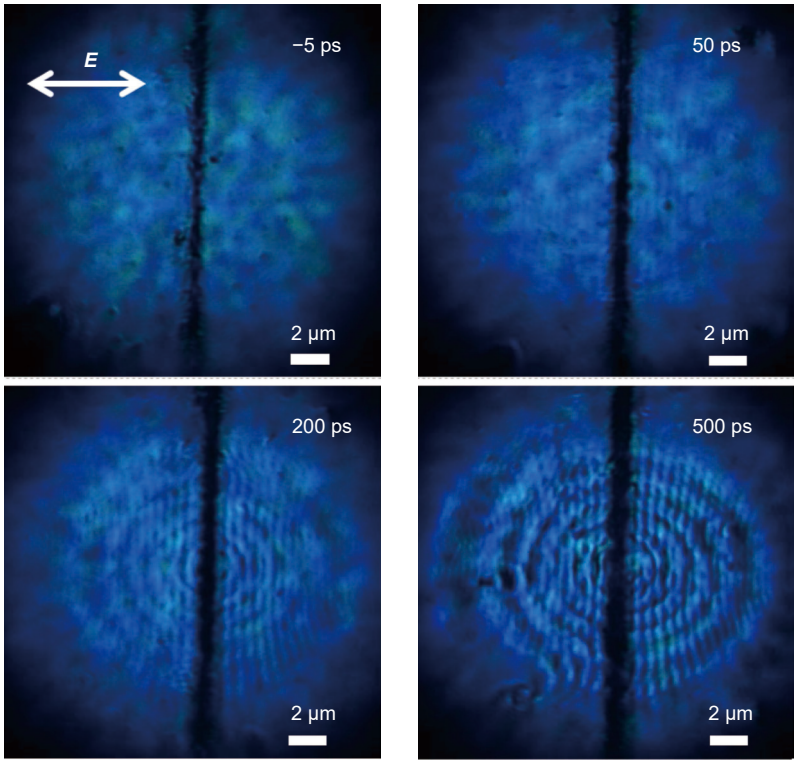

Fig. 6 | Evolution of LSFLs formed on Au film irradiated by a single 800 nm laser pulse with a fluence of 1.96 J/cm². The laser polarization, ***E***, is perpendicular to the prefabricated nanogroove. Figure reproduced with permission from ref.[25], American Physical Society.

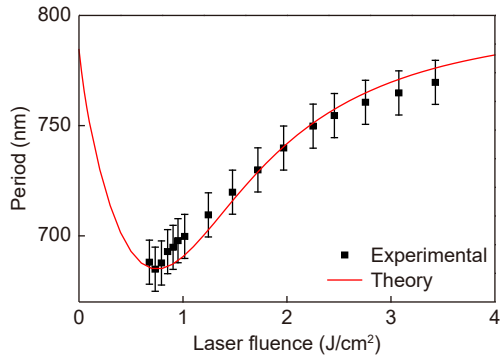

Fig. 7 | LSFL periods as a function of laser fluence *F*. The black squares and error bars show the experimental data, and the red curve shows the theoretical values. Figure reproduced with permission from ref.[25], American Physical Society.

further increased to 2.5 J/cm², the LSFL period increased to 756 nm. The developed SPP model accorded well with the experimental results, indicating that SPP excitation was the key during the formation of LSFLs on metal surfaces.

The electronic band structures and optical properties of Ag and Ni are significantly different, and can represent noble and common metals, respectively. The dependence of the transient LSFL periods of Ag and Ni films on the laser fluence was studied using the collinear pump-probe imaging method[56]. The experimental results agreed well with the theoretical values based on the developed SPP theory. Thus, the developed SPP model explains the formation mechanism of LSFLs on different types of metal surfaces.

Noncollinear pump-probe imaging techniques have also been applied to observe the formation of LSFLs. Murphy et al. reported the formation of LSFLs on silicon irradiated with multiple pulses[100]. Using optical diffraction microscopy, Kafka et al. detected the formation of LSFLs on Cu films irradiated with a single femtosecond pulse[54]. Garcia-Lechuga et al. used a moving-spot multiple-pulse irradiation approach, and observed the birth and growth of individual ripples on a silicon surface[101]. It was demonstrated that the formation of LIPSs was initiated by free carrier generation, leading to non-thermal melting, liquid-phase overheating, and rapid solidification into the amorphous phase.

Efficient fabrication of high-quality LIPSs with shaped ultrafast laser pulses

Temporally shaped ultrafast laser-induced high-quality LIPSs

To efficiently fabricate uniform and regular LIPSs, three main challenges should be addressed: enhancement of periodic deposition of laser energy, reduction of residual

heat, and avoidance of debris deposited on the ablation spots[8]. A temporally shaped ultrafast laser is an efficient tool for fabricating regular LIPSs[102]. By changing the sub-pulse interval, pulse number, and sub-pulse energy distribution of the burst pulse train, the regularity and uniformity of LIPSs were obviously improved, and the structural color was more vivid[103,104].

Double temporally delayed femtosecond laser beams can efficiently induce uniform LSFLs in semiconductors, metals and dielectrics[105,106]. A femtosecond laser was further shaped into symmetrical three- and four-pulse sequences for the fabrication of double-grating structures and HSFLs on fused silica[107].

By controlling the voltage of each element of the spatial light modulator (SLM) via computer programming, the phase and/or amplitude of the laser spectrum can be modulated, and the 4f zero-dispersion pulse-shaping system can generate shaped laser pulses with arbitrary temporal distributions[8]. Specifically, the number of sub-pulses, interval between adjacent subpulses, and pulse energy of each subpulse can be flexibly adjusted.

Regular LSFLs on silicon were processed using a 4f configuration zero-dispersion pulse-shaping system[8]. A Gaussian pulse is shaped into pulse trains with an interval of 16.2 ps by using periodic π-phase step modulation. The transient LIPSs started appearing on the Si surface at a delay time of 4 ps[52], which was shorter than the interval between adjacent sub-pulses. Thus, the transient LIPSs have started to appear under the illumination of the two main subpulses. When the subsequent subpulse reached the sample surface, the transient LIPSs induced by the previous subpulses enhanced the excitation of the SPPs, as well as the periodic distribution of the laser field.

When the subsequent small sub-pulses reached, the surface layer remained at a very high temperature. It was further excited and partially ablated, taking away some of the remaining heat (ablative cooling effect). Moreover, the ablated plume was further excited by the subsequent subpulses, and the debris was further ionized and vaporized, resulting in fewer deposited particles. Therefore, regular and uniform LSFLs were induced on the Si surface using a shaped pulse of 16.2 ps[8], as shown in Fig. 8.

The fabrication efficiency, depth, and regularity of the LSFLs when using shaped pulses of 16.2 ps were significantly better than those using Gaussian femtosecond laser pulses[8]. The scan velocity for fabricating regular LSFLs was 2.3 times faster, while the LSFLs depth was 2 times deeper, and the diffraction efficiency was 3 times higher than that of LSFLs using Gaussian femtosecond laser pulses.

Spatially shaped femtosecond laser-induced LIPSs with high efficiency

Arbitrary spatial intensity distribution of femtosecond laser pulses can be modulated by loading a computer-generated hologram (CGH) on a SLM, and LIPSs can be processed in parallel with high efficiency[108]. For example, Hayasaki et al. successfully realized the parallel processing of microstructures by loading a mixed-phase Fresnel lens on the SLM[109,110].

Maskless flexible spatial shaping based on spatiotemporal interference can modulate the interference intensity distribution into arbitrary patterns[111]. It was verified using a Michelson interferometer, where the phase of one laser beam was controlled via SLM.

Lin et al. developed a correction method for the spatial distortion and light intensity, which could greatly improve the accuracy of the spatial pattern and uniformity of the light intensity simply by changing the phase map loaded on the SLM[112]. This method was used to efficiently process colorful two-dimensional codes on silicon and shark-skin-like structures with superhydrophobic properties on stainless steel[112,113].

The laser focal point of a cylindrical lens is only a few to tens of micrometers wide, while its length is on the order of 1–10 mm[114,115]. Compared with ordinary circular lenses, the efficiency of femtosecond-LIPSs can be improved by a factor of 10^3–10^4 by using cylindrical lenses, which have been demonstrated in materials such as silicon and graphene oxide[11,57,116–118]. This method is very simple, and has important implications for the industrial application of femtosecond-LIPSs in the future.

Polarization shaped femtosecond-LIPSs

By using a liquid crystal SLM and/or Q-plate, a femtosecond Gaussian laser beam could be modulated into vortex light, radially polarized or angularly polarized beam[119–122], and used to directly fabricate complex LIPS patterns[77,121–129]. Two laser beams with s and p polarizations were collinearly focused on the SiC surface, and nanostructures with different morphologies were fabricated by adjusting the energy ratio of these two laser beams[77]. Radially and angularly polarized femtosecond lasers were focused on transparent materials and HSFL patterns consistent with the polarization distribution were fabricated[125].

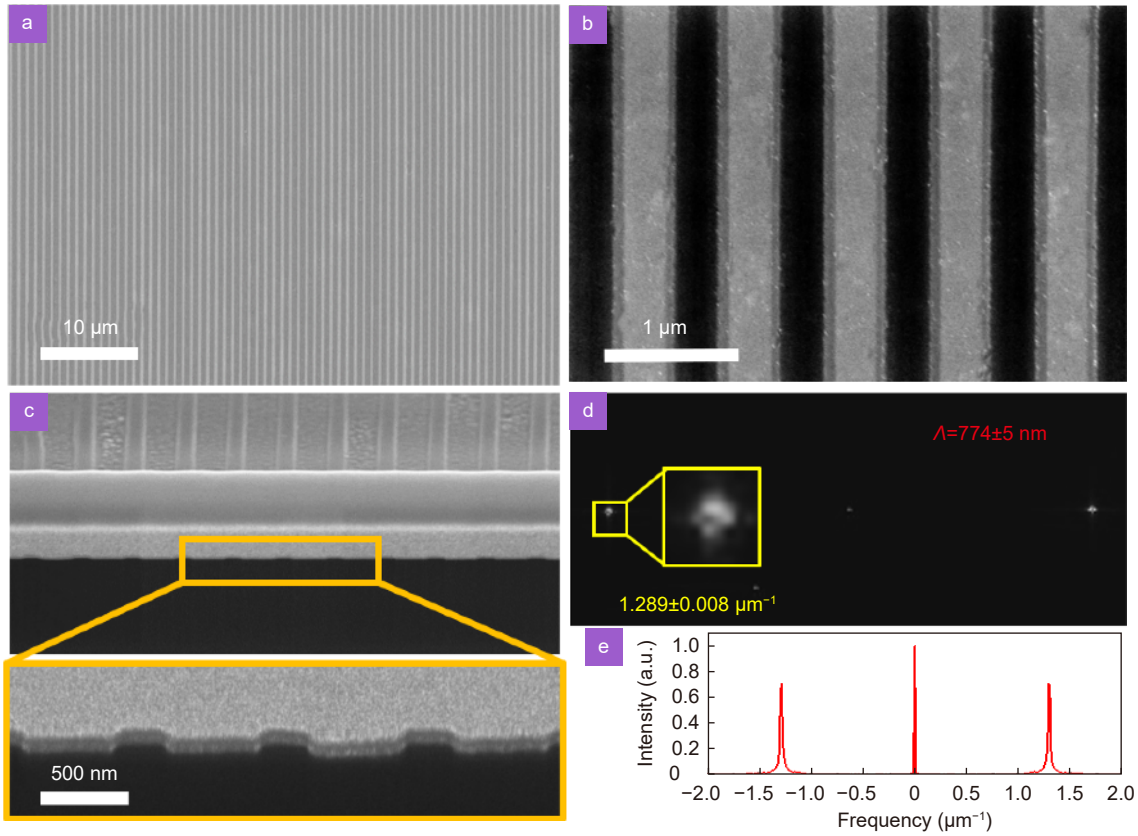

Fig. 8 | (**a**–**b**) SEM pictures of LSFLs induced by the shaped pulse trains with an interval of 16.2 ps. (**c**) The cross section of LSFLs. (**d**) The 2D fast Fourier transform of (b). (**e**) Spectra of the 2D Fourier transform along the *x*-axis. Figure reproduced with permission from ref.[8], Optica Publishing Group, under the Optica Open Access Publishing Agreement.

Efficient fabrication of complex femtosecond-LIPS patterns by multi-beam interference

Multibeam interference is an efficient etching technology for processing regular periodic patterns, where the light intensity distribution in the interference field is usually imprinted on the materials. By combining laser interference technology with femtosecond-LIPSs, many complex LIPS patterns were fabricated with high efficiency and quality by simultaneously controlling the light intensity distribution and polarization distribution[37,130]. Experimental and theoretical results showed that the longer-period structure was determined by the intensity distribution, whereas the LIPS pattern was determined by the polarization distribution[131].

Two-beam femtosecond laser interference was used to fabricate grating structures. By changing the laser polarization direction, interesting complex periodic structures covered with LIPSs have been efficiently fabricated[130,132]. Recently, large-area regular LSFLs were efficiently fabricated on a silicon wafer using double-beam femtosecond laser interference focused by cylindrical lens. The space of the double-beam interference fringes was an integer multiple of the SPP wavelength, thereby effectively exciting the resonance-enhanced SPPs. The fabricated nanogratings were very regular, uniform, and smooth, and the resolution of the diffraction light was almost the same as that with commercial gold gratings[57]. Using a similar method, a large area of regular and uniform LIPSs was processed on the surface of quartz glass[118].

A wide variety of composite LIPSs such as hexagonally distributed nanogratings, hexagonal nanoflowers, and nanorings were efficiently fabricated on wide-bandgap SiC and ZnO semiconductors by changing the polarization combination of the three beams[37,131], as shown in Fig. 9. The four-beam interference method was further developed, and composite LIPSs such as square nanostructures, symmetric petal structures, and asymmetric helix-like structures were prepared on the surface of a ZnO crystal[133].

Femtosecond laser direct writing of <100 nm nanostructures

Because of the diffraction limit, the size of the laser focus is typically a few hundred nanometers. The resolution of

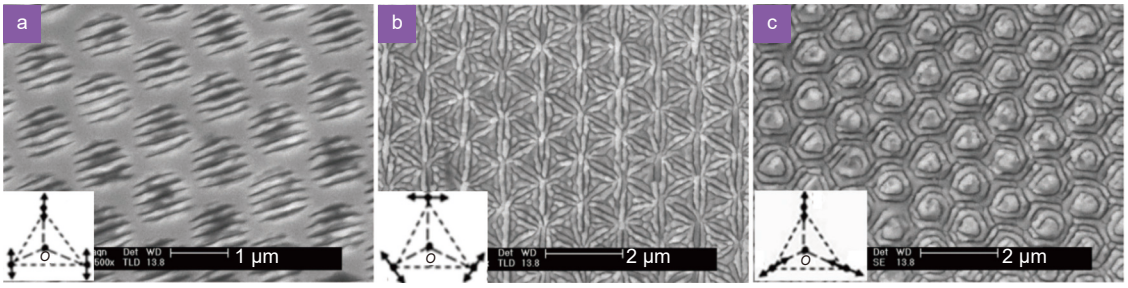

Fig. 9 | SEM images of composite LIPSs prepared by three-beam interference. The insets show the polarization combinations of the three laser beams. Figure reproduced with permission from ref.[37], under a Creative Commons Attribution 4.0 International License.

laser processing with high numerical aperture objectives is also on the order of hundreds of nanometers. The groove widths of HSFLs on semiconductor, dielectric, and metal surfaces induced by a femtosecond laser are typically less than 50 nm and less than 1/10 of the laser wavelength, opening up new avenues for laser processing with feature sizes smaller than 100 nm[134–138]. Liao et al. reported a single nanohollow channel with a width of 40 nm in porous glass using femtosecond laser-induced HSFL technology. It was used in nanofluidics in the field of single-molecule detection and biochip preparation. By precisely controlling the laser focus, fluences, and scanning speed, straight nanogrooves with widths smaller than 100 nm were prepared on the surfaces of fused silica and sapphire crystals[135].

A single nanogroove with a width of 30 nm and a double-groove structure with an interval of 150 nm were fabricated on a ZnO crystal surface immersed in water by precisely controlling the 800-nm femtosecond laser fluence and scanning speed[136], as shown in Fig. 10. Double-groove grating structures and single-groove grating structures with different spacings were fabricated, with groove depths ranging from 200 to 300 nm and groove widths smaller than 40 nm. Nanosquare structures with dimensions of 150 nm × 150 nm and 150 nm × 250 nm were fabricated by direct writing twice along the vertical direction.

By controlling the laser polarization always perpendicular to the scanning direction, curved nanogrooves with widths smaller than 20 nm and curvature radii smaller than 100 nm were fabricated on a silicon surface[139]. Lin et al. processed curved nanogrooves with a feature size of 12 nm on silicon surfaces using 800 nm femtosecond laser direct writing with orthogonally polarized dual beams[27].

Applications of LIPSs

Femtosecond-LIPSs provide a mask-free, high-efficiency processing method for tuning material properties. This method has been used in many fields, with applications that include structural colors[8,32,35], birefringent optical components[34,36,38], optical absorption and luminescence[33,37,39], and electrical properties[40].

Structural colors

Structural colors originate from the interference, diffraction, or scattering produced by micro/nanostructures on the surface of a material[32]. LIPSs have been widely used to produce structural colors on metals, semiconductors and transparent materials[8,35,118,140–151].

The properties of such structural colors are determined by the period, depth, and orientation of the LIPSs. LIPSs with periods in the range of 400 – 1500 nm were prepared on the surface of stainless steel using femtosecond lasers with different wavelengths[140]. These LIPSs demonstrated completely different colors under each diffraction order, such that the structural color of the stainless steel surface could cover most of the color gamut. The same LIPSs displayed different colors at different angles[118,142,148]. Therefore, surfaces with different colors were prepared by controlling the orientation of the LIPSs. Liu et al. proposed to control the orientation of LIPSs in real time using a femtosecond laser double-pulse sequence with orthogonal polarization and equal pulse energy and fabricated LIPSs with arbitrary orientations on silicon surfaces that were not affected by the scanning path[147]. This is of great significance for multi-layer encryption, anti-counterfeiting, and so on.

The brightness and purity of the structural colors were affected by the regularity and depth of the LIPSs. The high-efficiency preparation of high-quality LIPSs has attracted increasing attention. Zhang et al.[8] fabricated very regular and deep LSFLs on a silicon surface using temporally shaped pulses via a 4f zero-dispersion system and demonstrated very bright and pure structural colors, as shown in Fig. 11. Vivid structural colors on fused silica surfaces were prepared with high efficiency using the double-beam interference of femtosecond laser focused

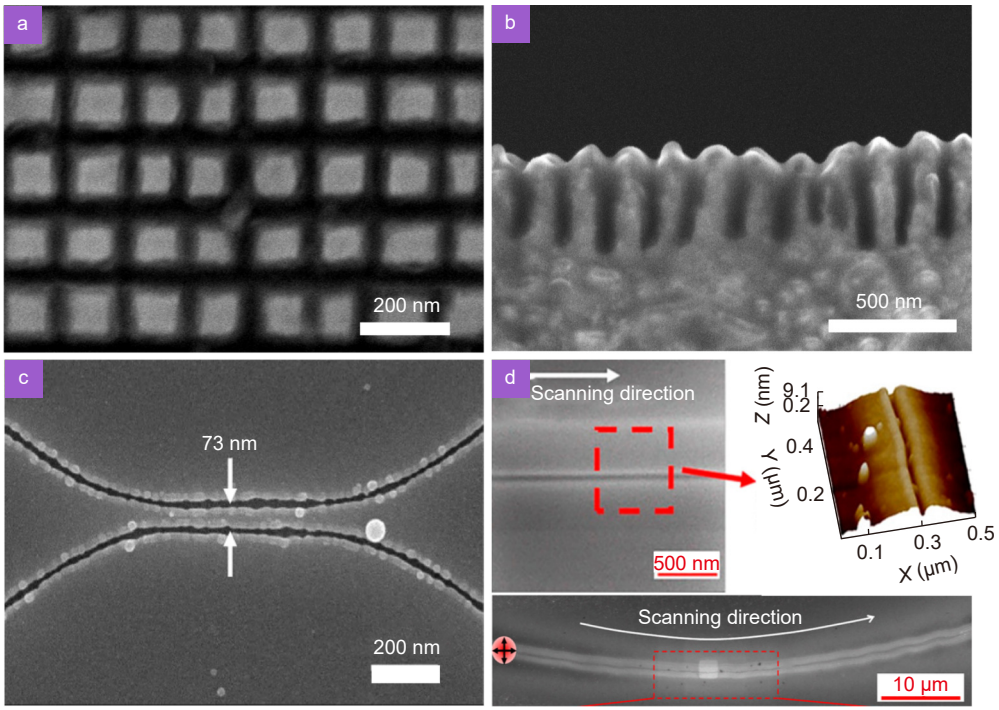

Fig. 10 | (**a**) SEM images of nanosquares , and (**b**) the cross section of nanogratings . (**c**) Curvature and separation control of nanogrooves fabricated by 800 nm femtosecond laser with polarization control. (**d**) SEM and AFM images of curved single nanogroove on silicon surface induced by 800 nm femtosecond laser with orthogonally polarized dual beams. Figure reproduced with permission from: (a, b) ref.[136], under Optica Open Access Publishing Agreement; (c) ref.[139], under a Creative Commons Attribution 4.0 International License; (d) ref.[27], American Chemical Society.

Fig. 11 | Structural colors of "Chinese knot" pattern made up of LSFLs fabricated by a shaped pulse of 16.2 ps on Si surface under different diffraction angles. The inset shows an SEM image of regular LSFLs. Figure reproduced with permission from ref.[8], Optica Publishing Group, under the Optica Open Access Publishing Agreement.

by cylindrical lens[118]. Chemical etching-assisted LIPSs are also an effective method for producing bright structural colors[148,150].

Birefringent optical components and information storage

HSFL nanostructures inside fused silica exhibit birefringence effects comparable to those of quartz crystals[34,36,152,153] and have been used in the storage of multi-dimensional data, as shown in Fig. 12. Zhang et al.[154] demonstrated that HSFLs could encode the intensity and polarization state of light at multiple levels and successfully retrieved digital files that were optically encrypted into five dimensions. Experiments indicated that HSFLs in silica glass have high stability and rewritability, meeting some requirements for developing high-density data storage[38]. Recently, Wang et al. demonstrated 100-layer 5D optical data storage based on femtosecond laser-induced birefringence with a high readout accuracy and no bit error rates[155] , as shown in Fig. 12. At present, the limitations of optical storage technology lie mainly in efficient writing and fast and accurate reading.

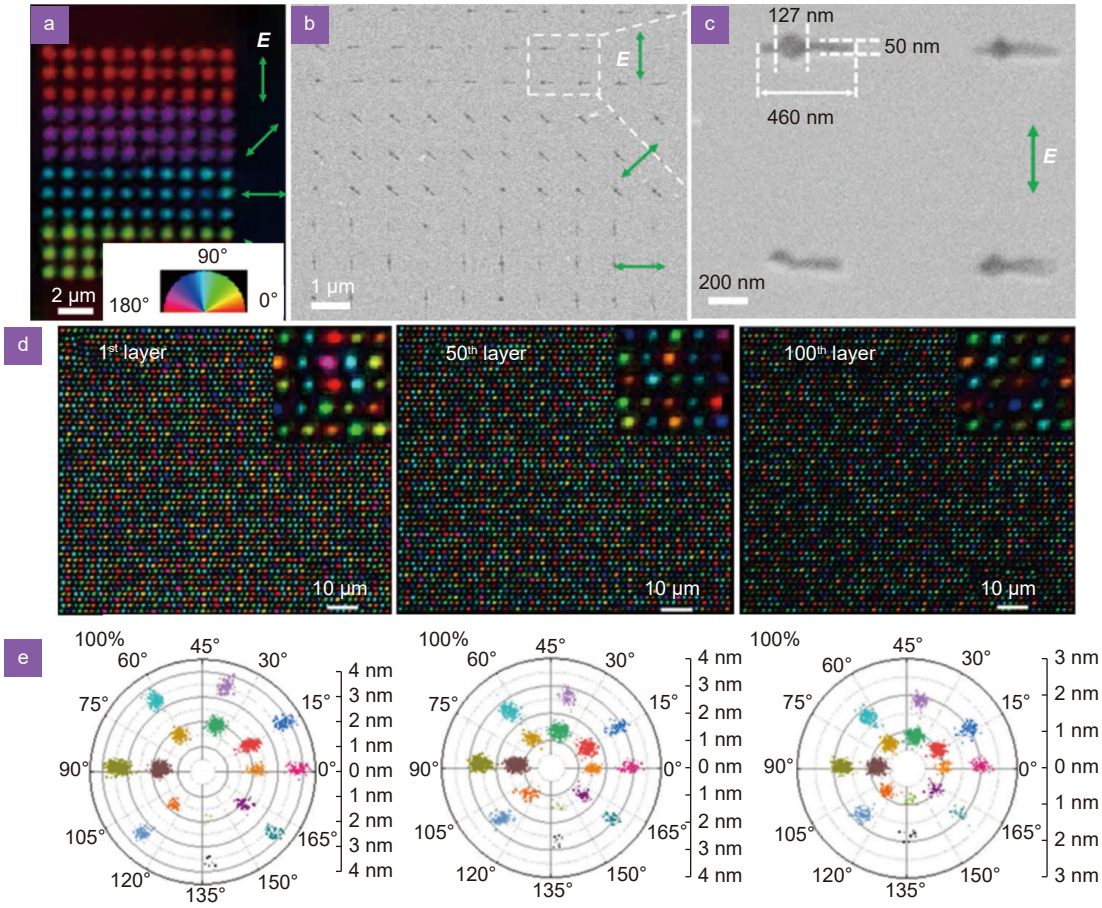

Fig. 12 | (**a**-**c**) Imaging of anisotropic nanostructures and 5D optical data storage in fused silica[153,155]. (**a**) Image of the slow axis azimuth of voxels, where the pseudo-color represents the slow axis azimuth. (**b**) SEM image of the nanolamella-like structure after polishing and KOH etching. (**c**) The enlarged area in the dashed square in (b). (**d**) The birefringent images of data voxels of different layers in a 100-layer 5D optical data storage in fused silica after removing the background. Insets are enlargements of small region (10 μm × 10 μm). (**e**) Polar diagram of the measured retardance and azimuth of all voxels in (d). Figure reproduced with permission from: (a-c) ref.[153], Optica Publishing Group, under the Optica Open Access Publishing Agreement; (d, e) ref.[155], under a Creative Commons Attribution License.

The writing speed has been increased to 225 kB/s[153–155], which is mainly a result of the higher laser power and repetition frequency with pulse energy modulation, as shown in Fig. 12.

Mechanisms and applications based on femtosecond laser-induced birefringence have been extensively studied, including various polarization-sensitive elements[70,156–158] such as polarization beam splitters[159], polarization diffraction gratings[160], and polarization optical vortex rotation converters[123]. HSFLs fabricated in amorphous silicon[161,162], silicon carbide[163] and indium tin oxide (ITO) thin films[164,165] exhibit birefringence effects two orders of magnitude higher than those of quartz glass, demonstrating that high-refractive-index materials can be used to fabricate birefringent elements. Large-area HSFLs have been efficiently fabricated on a glass surface coated with an ITO thin film using femtosecond laser direct writing focused via a cylindrical lens[166]. The optical retardation reached 44 nm, which was eight times that of the HSFLs processed directly on a bare glass surface.

Enhancement of optical absorption and photoluminescence

The optical properties were significantly tuned after forming complex micro-nanostructures covered with LIPSs on the surfaces of metals, semiconductors, and dielectrics[33,35,37,39,118,167–174]. “Black” silicon has been extensively studied and was shown to exhibit ultra-low reflectivity and very high absorption in the UV–NIR region as a result of nanostructures fabricated by femtosecond lasers[33,39,171,172].

Various composite LIPSs have been efficiently fabricated on wide-bandgap SiC and ZnO semiconductors by the multi-beam interference of femtosecond lasers[174,176].

These composite nanostructures exhibited greatly enhanced light absorption in the UV–NIR region, as well as an intense blue emission when excited by infrared femtosecond lasers. Compared with the smooth surface of ZnSe crystals, the blue light intensity of the composite nanostructures excited by a 1200 nm femtosecond laser was enhanced by 30–100 times[175], as shown in Fig. 13.

Electrical properties improved by LIPSs

Recently, the effect of LIPSs on the electrical properties of ITO[40,41,177] and the superconducting material niobium[178,179] has received increasing attention. ITO films are widely used as transparent conductive materials in solar cells, sensors, and displays. An ITO film with LIPSs exhibited good anisotropic conductivity and, if fabricated under appropriate conditions, could even achieve unidirectional conductivity, as shown in Fig. 14[41]. Moreover, the transmittance in the near-infrared region was greatly enhanced[40,41,177]. These results demonstrate the potentials of femtosecond LIPSs for efficiently fabricating large-scale transparent nanowires[180].

Cubero et al.[178,179] analyzed the effect of laser irradiation on the critical current value of superconductors by measuring hysteresis loops, and proved that LIPSs could change the superconducting properties of niobium. The secondary electron emission from a copper surface with LIPSs was effectively reduced[181], which was very effective in suppressing secondary electron emission in accelerators.

Other applications

After femtosecond laser processing, the entire ablation area is covered with nanostructures, which can effectively increase the surface roughness and reduce the contact area with the droplet. This is an efficient method to alter the hydrophilicity and hydrophobicity of sample surfaces, and has been successfully demonstrated on various materials including metals, semiconductors, dielectrics, and polymers[182–192].

Femtosecond-LIPSs were optimized on steel, titanium alloy, and atomic layer deposition cemented carbide surfaces. The friction coefficient and the wear were reduced significantly, which revealed the great potential for tribological applications[193–199].

Outlook

In this paper, the formation mechanisms, high-quality and high-efficiency processing methods, and applications of LIPSs were reviewed. We believe that the following problems that may be worth further investigation.

Formation mechanisms of LIPSs

The formation mechanism of LIPSs has always been a hot topic in this field. The scattered light model and propagating SPP model are continuously being developed and refined and have been used to explain the formation of LSFLs on dielectrics, semiconductors, and metals. However, the formation mechanism of LSFLs requires further experimental and theoretical studies, especially ultrafast dynamics.

HSFLs are typically formed after irradiation with multiple pulses. Their formation mechanism is more complex and difficult to determine than that of LSFLs, requiring extensive experimental and theoretical studies, including numerical simulations of the dynamics using the COMSOL and FDTD methods. In recent years,

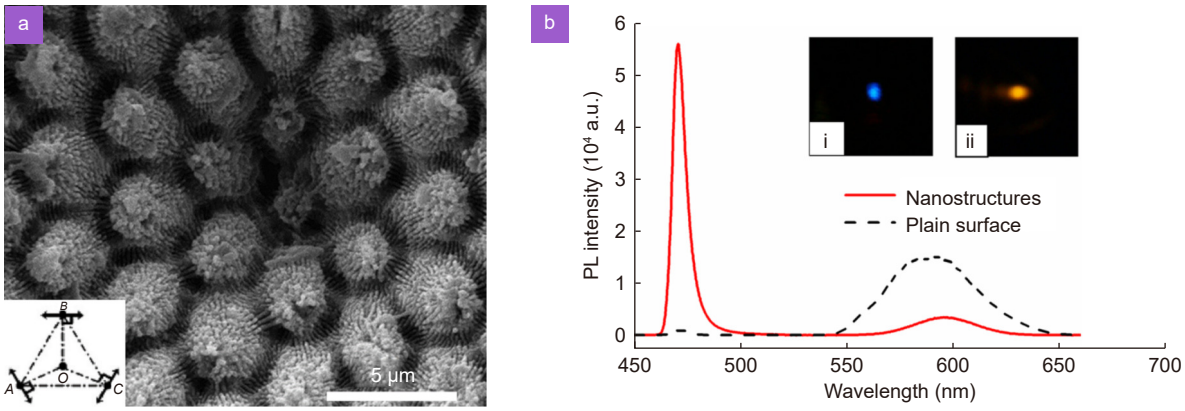

Fig. 13 | (**a**) SEM image of composite nanostructures on ZnSe crystal. (**b**) The photoluminescence (PL) spectra of the plane surface and composite nanostructures irradiated by 1200 nm femtosecond laser. Insets (i) and (ii) show PL images of the nanostructures and plane surface, respectively. Figure reproduced with permission from ref.[175], AIP Publishing.

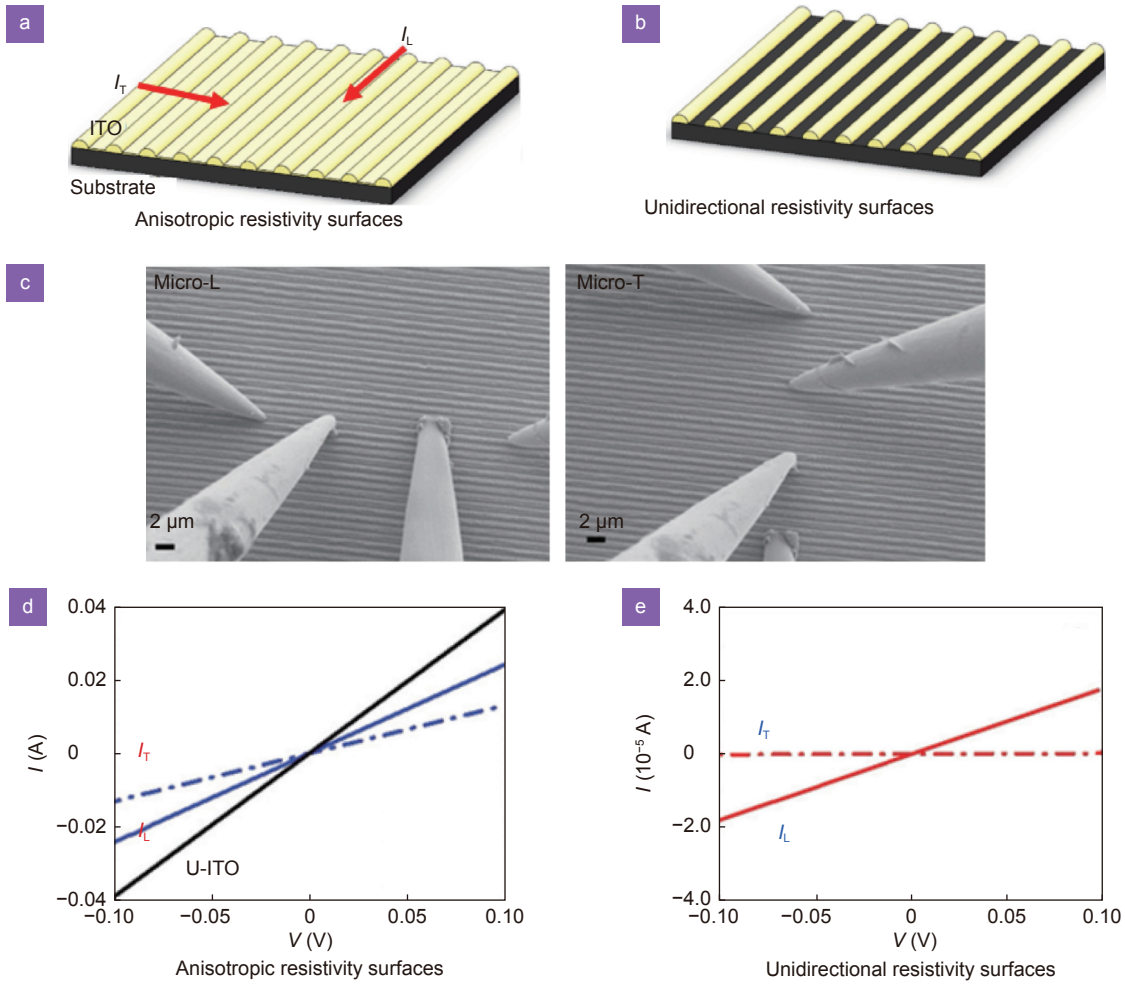

Fig. 14 | (**a**–**b**) Schematic illustrations of the laser-induced structure in the ITO thin film on the substrate, and the resistivity measured longitudinally (I_L) or transversely (I_T) along the LIPS direction. (**c**) Microscopic configuration of the four-point probe measurement with the probes longitudinal (Micro-L) or transverse (Micro-T) aligned with the LIPSs. (**d**) and (**e**) are the *I*-*V* curves of the anisotropic resistivity surface and the unidirectional resistivity surface measured by the Micro-L or Micro-T method, respectively. Figure reproduced with permission from ref.[41], under a Creative Commons Attribution License.

various far-field super-resolution imaging methods have been reported[200–202]. Combining the pump-probe method with far-field super-resolution imaging is very interesting and may be helpful in revealing the formation mechanism of HSFLs irradiated by a femtosecond laser.

Patterns with features of <30 nm obtained by direct writing

The groove width of HSFLs is only tens of nanometers, which provides a new method of nanofabrication using ultrafast laser direct writing. However, before this can be widely applied, there are still many problems to be solved such as the slow scanning speed and poor uniformity of the nanogrooves. In the last decade, multi-dimensional laser shaping technologies in time/frequency and polarization have been rapidly developed[108,203]. Synchronizing laser direct writing and multi-dimensional laser shaping in real time will ensure that the nanogrooves grow along the direction of the direct laser writing, improve the local optical field enhancement, and reduce the residual heat of ablation. This is expected to efficiently fabricate high-quality nanopatterns with features less than 30 nm.

LIPSs based on multi-dimensional laser shaping and its applications

Large-area LIPSs fabricated with high quality, efficiency, and stability can greatly promote their applications in many fields. By developing pulse-shaping methods based on the 4f configuration zero-dispersion system or Fabry-Perot interferometer[204], the regularity and depth of LIPSs can be effectively improved, which will improve the phase retardation and writing speed and reduce the bit

error rate when reading out. Combining time/frequency shaping and spatial shaping can improve the regularity and depth of LIPSs fabricated with high efficiency, thereby improving the purity and brightness of the structural colors. By simultaneously controlling the polarization and spatial distribution of the laser field, nanostructures with designed patterns and specific nanogroove distributions can be processed with high efficiency. Combining time/frequency domain shaping and polarization shaping can improve the quality and efficiency of far-field nanofabrication and allow LIPS applications in new fields such as metasurfaces and microelectronics.

References

1. Fork RL, Greene BI, Shank CV. Generation of optical pulses shorter than 0.1 psec by colliding pulse mode locking. *Appl Phys Lett* **38**, 671–672 (1981).
2. Chichkov BN, Momma C, Nolte S, Von Alvensleben F, Tünnermann A. Femtosecond, picosecond and nanosecond laser ablation of solids. *Appl Phys A* **63**, 109–115 (1996).
3. Sugioka K, Cheng Y. Ultrafast lasers—reliable tools for advanced materials processing. *Light Sci Appl* **3**, e149 (2014).
4. Buividas R, Mikutis M, Juodkazis S. Surface and bulk structuring of materials by ripples with long and short laser pulses: recent advances. *Prog Quant Electron* **38**, 119–156 (2014).
5. Yang QX, Liu HL, He S, Tian QY, Xu B et al. Circular cladding waveguides in Pr:YAG fabricated by femtosecond laser inscription: Raman, luminescence properties and guiding performance. *Opto-Electron Adv* **4**, 200005 (2021).
6. Wang HT, Hao CL, Lin H, Wang YT, Lan T et al. Generation of super-resolved optical needle and multifocal array using graphene oxide metalenses. *Opto-Electron Adv* **4**, 200031 (2021).
7. Zhang YC, Jiang QL, Cao KQ, Chen TQ, Cheng K et al. Extremely regular periodic surface structures in a large area efficiently induced on silicon by temporally shaped femtosecond laser. *Photonics Res* **9**, 839–847 (2021).
8. Jia TQ, Chen HX, Huang M, Zhao FL, Qiu JR et al. Formation of nanogratings on the surface of a ZnSe crystal irradiated by femtosecond laser pulses. *Phys Rev B* **72**, 125429 (2005).
9. Wang JC, Guo CL. Ultrafast dynamics of femtosecond laser-induced periodic surface pattern formation on metals. *Appl Phys Lett* **87**, 251914 (2005).
10. Wang L, Chen QD, Cao XW, Buividas R, Wang XW et al. Plasmonic nano-printing: large-area nanoscale energy deposition for efficient surface texturing. *Light Sci Appl* **6**, e17112 (2017).
11. Miyaji G, Miyazaki K, Zhang KF, Yoshifuji T, Fujita J. Mechanism of femtosecond-laser-induced periodic nanostructure formation on crystalline silicon surface immersed in water. *Opt Express* **20**, 14848–14856 (2012).
12. Xie HB, Zhao B, Cheng JL, Chamoli SK, Zou TT et al. Super-regular femtosecond laser nanolithography based on dual-interface plasmons coupling. *Nanophotonics* **10**, 3831–3842 (2021).
13. Gnilitskyi I, Derrien TJY, Levy Y, Bulgakova NM, Mocek T et al. High-speed manufacturing of highly regular femtosecond laser-induced periodic surface structures: physical origin of regularity. *Sci Rep* **7**, 8485 (2017).
14. Boneberg J, Leiderer P. Optical near-field imaging and nanostructuring by means of laser ablation. *Opto-Electron Sci* **1**, 210003 (2022).
15. Birnbaum M. Semiconductor surface damage produced by ruby lasers. *J Appl Phys* **36**, 3688–3689 (1965).
16. Sipe JE, Young JF, Preston JS, Van Driel HM. Laser-induced periodic surface structure. I. Theory. *Phys Rev B* **27**, 1141–1154 (1983).
17. Shimotsuma Y, Kazansky PG, Qiu JR, Hirao K. Self-organized nanogratings in glass irradiated by ultrashort light pulses. *Phys Rev Lett* **91**, 247405 (2003).
18. Bonse J, Munz M, Sturm H. Structure formation on the surface of indium phosphide irradiated by femtosecond laser pulses. *J Appl Phys* **97**, 013538 (2005).
19. Miyaji G, Miyazaki K. Ultrafast dynamics of periodic nanostructure formation on diamondlike carbon films irradiated with femtosecond laser pulses. *Appl Phys Lett* **89**, 191902 (2006).
20. Bhardwaj VR, Simova E, Rajeev PP, Hnatovsky C, Taylor RS et al. Optically produced arrays of planar nanostructures inside fused silica. *Phys Rev Lett* **96**, 057404 (2006).
21. Huang M, Zhao FL, Cheng Y, Xu NS, Xu ZZ. Origin of laser-induced near-subwavelength ripples: interference between surface plasmons and incident laser. *ACS Nano* **3**, 4062–4070 (2009).
22. Höhm S, Rosenfeld A, Krüger J, Bonse J. Femtosecond laser-induced periodic surface structures on silica. *J Appl Phys* **112**, 014901 (2012).
23. Bonse J, Krüger J, Höhm S, Rosenfeld A. Femtosecond laser-induced periodic surface structures. *J Laser Appl* **24**, 042006 (2012).
24. Reif J, Varlamova O, Uhlig S, Varlamov S, Bestehorn M. On the physics of self-organized nanostructure formation upon femtosecond laser ablation. *Appl Phys A* **117**, 179–184 (2014).
25. Cheng K, Liu JK, Cao KQ, Chen L, Zhang YC et al. Ultrafast dynamics of single-pulse femtosecond laser-induced periodic ripples on the surface of a gold film. *Phys Rev B* **98**, 184106 (2018).
26. Rudenko A, Mauclair C, Garrelie F, Stoian R, Colombier JP. Self-organization of surfaces on the nanoscale by topography-mediated selection of quasi-cylindrical and plasmonic waves. *Nanophotonics* **8**, 459–465 (2019).
27. Lin ZY, Liu HG, Ji LF, Lin WX, Hong MH. Realization of ~10 nm features on semiconductor surfaces via femtosecond laser direct patterning in far field and in ambient air. *Nano Lett* **20**, 4947–4952 (2020).
28. Tsibidis GD, Fotakis C, Stratakis E. From ripples to spikes: a hydrodynamical mechanism to interpret femtosecond laser-induced self-assembled structures. *Phys Rev B* **92**, 041405(R) (2015).
29. Vorobyev AY, Guo CL. Direct femtosecond laser surface nano/microstructuring and its applications. *Laser Photonics Rev* **7**, 385–407 (2013).
30. Fraggelakis F, Mincuzzi G, Lopez J, Manek-Hönninger I, Kling R. Controlling 2D laser nano structuring over large area with double femtosecond pulses. *Appl Surf Sci* **470**, 677–686

(2019).
31. Zhang DS, Li XZ, Fu Y, Yao QH, Li ZG et al. Liquid vortexes and flows induced by femtosecond laser ablation in liquid governing formation of circular and crisscross LIPSS. *Opto-Electron Adv* **5**, 210066 (2022).
32. Parker AR. 515 million years of structural colour. *J Opt A Pure Appl Opt* **2**, R15–R28 (2000).
33. Wu C, Crouch CH, Zhao L, Carey JE, Younkin R et al. Near-unity below-band-gap absorption by microstructured silicon. *Appl Phys Lett* **78**, 1850–1852 (2001).
34. Bricchi E, Klappauf BG, Kazansky PG. Form birefringence and negative index change created by femtosecond direct writing in transparent materials. *Opt Lett* **29**, 119–121 (2004).
35. Vorobyev AY, Guo CL. Colorizing metals with femtosecond laser pulses. *Appl Phys Lett* **92**, 041914 (2008).
36. Shimotsuma Y, Sakakura M, Kazansky PG, Beresna M, Qiu JR et al. Ultrafast manipulation of self-assembled form birefringence in glass. *Adv Mater* **22**, 4039–4043 (2010).
37. Xiong PX, Jia TQ, Jia X, Feng DH, Zhang SA et al. Ultraviolet luminescence enhancement of ZnO two-dimensional periodic nanostructures fabricated by the interference of three femtosecond laser beams. *New J Phys* **13**, 023044 (2011).
38. Gu M, Li XP, Cao YY. Optical storage arrays: a perspective for future big data storage. *Light Sci Appl* **3**, e177 (2014).
39. Crouch CH, Carey JE, Shen M, Mazur E, Génin FY. Infrared absorption by sulfur-doped silicon formed by femtosecond laser irradiation. *Appl Phys A* **79**, 1635–1641 (2004).
40. Solodar A, Cerkauskaite A, Drevinskas R, Kazansky PG, Abdulhalim I. Ultrafast laser induced nanostructured ITO for liquid crystal alignment and higher transparency electrodes. *Appl Phys Lett* **113**, 081603 (2018).
41. Lopez-Santos C, Puerto D, Siegel J, Macias-Montero M, Florian C et al. Anisotropic resistivity surfaces produced in ITO films by laser-induced nanoscale self-organization. *Adv Opt Mater* **9**, 2001086 (2021).
42. Garrelie F, Colombier JP, Pigeon F, Tonchev S, Faure N et al. Evidence of surface plasmon resonance in ultrafast laser-induced ripples. *Opt Express* **19**, 9035–9043 (2011).
43. Tsibidis GD, Skoulas E, Papadopoulos A, Stratakis E. Convection roll-driven generation of supra-wavelength periodic surface structures on dielectrics upon irradiation with femtosecond pulsed lasers. *Phys Rev B* **94**, 081305(R) (2016).
44. Emmony DC, Howson RP, Willis LJ. Laser mirror damage in germanium at 10.6 μm. *Appl Phys Lett* **23**, 598–600 (1973).
45. Csete M, Marti O, Bor Z. Laser-induced periodic surface structures on different poly-carbonate films. *Appl Phys A* **73**, 521–526 (2001).
46. Austin DR, Kafka KRP, Lai YH, Wang Z, Zhang KK et al. High spatial frequency laser induced periodic surface structure formation in germanium by mid-IR femtosecond pulses. *J Appl Phys* **120**, 143103 (2016).
47. Bonse J, Höhm S, Kirner SV, Rosenfeld A, Krüger J. Laser-induced periodic surface structures-a scientific evergreen. *IEEE J Sel Top Quantum Electron* **23**, 9000615 (2017).
48. Bonse J, Rosenfeld A, Krüger J. On the role of surface plasmon polaritons in the formation of laser-induced periodic surface structures upon irradiation of silicon by femtosecond-laser pulses. *J Appl Phys* **106**, 104910 (2009).
49. Zhou K, Jia X, Jia TQ, Cheng K, Cao KQ et al. The influences of surface plasmons and thermal effects on femtosecond laser-induced subwavelength periodic ripples on Au film by pump-probe imaging. *J Appl Phys* **121**, 104301 (2017).
50. Gurevich EL, Gurevich SV. Laser induced periodic surface structures induced by surface plasmons coupled via roughness. *Appl Surf Sci* **302**, 118–123 (2014).
51. Liu JK, Jia TQ, Zhao HW, Huang YQ. Two-photon excitation of surface plasmon and the period-increasing effect of low spatial frequency ripples on a GaP crystal in air/water. *J Phys D Appl Phys* **49**, 435105 (2016).
52. Liu JK, Jia X, Wu WS, Cheng K, Feng DH et al. Ultrafast imaging on the formation of periodic ripples on a Si surface with a prefabricated nanogroove induced by a single femtosecond laser pulse. *Opt Express* **26**, 6302–6315 (2018).
53. Fuentes-Edfuf Y, Sánchez-Gil JA, Florian C, Giannini V, Solis J et al. Surface plasmon polaritons on rough metal surfaces: role in the formation of laser-induced periodic surface structures. *ACS Omega* **4**, 6939–6946 (2019).
54. Kafka KRP, Austin DR, Li H, Yi AY, Cheng J et al. Time-resolved measurement of single pulse femtosecond laser-induced periodic surface structure formation induced by a prefabricated surface groove. *Opt Express* **23**, 19432–19441 (2015).
55. Jia X, Jia TQ, Peng NN, Feng DH, Zhang SA et al. Dynamics of femtosecond laser-induced periodic surface structures on silicon by high spatial and temporal resolution imaging. *J Appl Phys* **115**, 143102 (2014).
56. Cheng K, Cao KQ, Zhang YC, Han RZ, Feng DH et al. Ultrafast dynamics of subwavelength periodic ripples induced by single femtosecond pulse: from noble to common metals. *J Phys D Appl Phys* **53**, 285102 (2020).
57. Cao KQ, Chen L, Wu HC, Liu JK, Cheng K et al. Large-area commercial-grating-quality subwavelength periodic ripples on silicon efficiently fabricated by gentle ablation with femtosecond laser interference via two cylindrical lenses. *Opt Laser Technol* **131**, 106441 (2020).
58. Derrien TJY, Itina TE, Torres R, Sarnet T, Sentis M. Possible surface plasmon polariton excitation under femtosecond laser irradiation of silicon. *J Appl Phys* **114**, 083104 (2013).
59. Tsibidis GD, Barberoglou M, Loukakos PA, Stratakis E, Fotakis C. Dynamics of ripple formation on silicon surfaces by ultrashort laser pulses in subablation conditions. *Phys Rev B* **86**, 115316 (2012).
60. Barberoglou M, Tsibidis GD, Gray D, Magoulakis E, Fotakis C et al. The influence of ultra-fast temporal energy regulation on the morphology of Si surfaces through femtosecond double pulse laser irradiation. *Appl Phys A* **113**, 273–283 (2013).
61. Tsibidis GD, Stratakis E, Loukakos PA, Fotakis C. Controlled ultrashort-pulse laser-induced ripple formation on semiconductors. *Appl Phys A* **114**, 57–68 (2014).
62. Miyaji G, Hagiya M, Miyazaki K. Excitation of surface plasmon polaritons on silicon with an intense femtosecond laser pulse. *Phys Rev B* **96**, 045122 (2017).
63. Wortmann D, Gottmann J, Brandt N, Horn-Solle H. Micro- and nanostructures inside sapphire by fs-laser irradiation and selective etching. *Opt Express* **16**, 1517–1522 (2008).
64. Gottmann J, Wortmann D, Hörstmann-Jungemann M.

Fabrication of sub-wavelength surface ripples and in-volume nanostructures by fs-laser induced selective etching. *Appl Surf Sci* **255**, 5641–5646 (2009).

65. Richter S, Miese C, Döring S, Zimmermann F, Withford MJ et al. Laser induced nanogratings beyond fused silica-periodic nanostructures in borosilicate glasses and ULE™. *Opt Mater Express* **3**, 1161–1166 (2013).
66. Hnatovsky C, Taylor RS, Rajeev PP, Simova E, Bhardwaj VR et al. Pulse duration dependence of femtosecond-laser-fabricated nanogratings in fused silica. *Appl Phys Lett* **87**, 014104 (2005).
67. Corbari C, Champion A, Gecevičius M, Beresna M, Bellouard Y et al. Femtosecond versus picosecond laser machining of nano-gratings and micro-channels in silica glass. *Opt Express* **21**, 3946–3958 (2013).
68. Taylor RS, Hnatovsky C, Simova E, Rajeev PP, Rayner DM et al. Femtosecond laser erasing and rewriting of self-organized planar nanocracks in fused silica glass. *Opt Lett* **32**, 2888–2890 (2007).
69. Juodkazis S, Nishimura K, Okuno H, Tabuchi Y, Matsuo S et al. Three-dimensional laser microfabrication of metals, semiconductors, and dielectrics. *Proc SPIE* **6732**, 67320B (2007).
70. Taylor R, Hnatovsky C, Simova E. Applications of femtosecond laser induced self-organized planar nanocracks inside fused silica glass. *Laser Photonics Rev* **2**, 26–46 (2008).
71. Liao Y, Pan WJ, Cui Y, Qiao LL, Bellouard Y et al. Formation of in-volume nanogratings with sub-100-nm periods in glass by femtosecond laser irradiation. *Opt Lett* **40**, 3623–3626 (2015).
72. Liao Y, Ni JL, Qiao LL, Huang M, Bellouard Y et al. High-fidelity visualization of formation of volume nanogratings in porous glass by femtosecond laser irradiation. *Optica* **2**, 329–334 (2015).
73. Nayak BK, Gupta MC. Ultrafast laser-induced self-organized conical micro/nano surface structures and their origin. *Opt Lasers Eng* **48**, 966–973 (2010).
74. Volkov SN, Kaplan AE, Miyazaki K. Evanescent field at nano-corrugated dielectric surface. *Appl Phys Lett* **94**, 041104 (2009).
75. Dong YY, Molian P. Coulomb explosion-induced formation of highly oriented nanoparticles on thin films of 3C-SiC by the femtosecond pulsed laser. *Appl Phys Lett* **84**, 10–12 (2004).
76. Huang M, Zhao FL, Cheng Y, Xu NS, Xu ZZ. Mechanisms of ultrafast laser-induced deep-subwavelength gratings on graphite and diamond. *Phys Rev B* **79**, 125436 (2009).
77. Jia TQ, Zhao FL, Huang M, Chen HX, Qiu JR et al. Alignment of nanoparticles formed on the surface of 6H-SiC crystals irradiated by two collinear femtosecond laser beams. *Appl Phys Lett* **88**, 111117 (2006).
78. Le Harzic R, Dörr D, Sauer D, Stracke F, Zimmermann H. Generation of high spatial frequency ripples on silicon under ultrashort laser pulses irradiation. *Appl Phys Lett* **98**, 211905 (2011).
79. Hou SS, Huo YY, Xiong PX, Zhang Y, Zhang SA et al. Formation of long- and short-periodic nanoripples on stainless steel irradiated by femtosecond laser pulses. *J Phys D Appl Phys* **44**, 505401 (2011).
80. Huang M, Cheng Y, Zhao FL, Xu ZZ. The significant role of plasmonic effects in femtosecond laser-induced grating fabrication on the nanoscale. *Ann Phys* **525**, 74–86 (2013).
81. Wang L, Xu BB, Cao XW, Li QK, Tian WJ et al. Competition between subwavelength and deep-subwavelength structures ablated by ultrashort laser pulses. *Optica* **4**, 637–642 (2017).
82. Miyazaki K, Miyaji G. Nanograting formation through surface plasmon fields induced by femtosecond laser pulses. *J Appl Phys* **114**, 153108 (2013).
83. Makin VS, Makin RS, Vorobyev AY, Guo CL. Dissipative nanostructures and Feigenbaum's universality in the "Metal-high-power ultrashort-pulsed polarized radiation" nonequilibrium nonlinear dynamical system. *Tech Phys Lett* **34**, 387–390 (2008).
84. Fuentes-Edfuf Y, Sánchez-Gil JA, Garcia-Pardo M, Serna R, Tsibidis GD et al. Tuning the period of femtosecond laser induced surface structures in steel: from angled incidence to quill writing. *Appl Surf Sci* **493**, 948–955 (2019).
85. Zhang H, Colombier JP, Li C, Faure N, Cheng GH et al. Coherence in ultrafast laser-induced periodic surface structures. *Phys Rev B* **92**, 174109 (2015).
86. Rahmani M, Lei DY, Giannini V, Lukiyanchuk B, Ranjbar M et al. Subgroup decomposition of plasmonic resonances in hybrid oligomers: modeling the resonance lineshape. *Nano Lett* **12**, 2101–2106 (2012).
87. Okamuro K, Hashida M, Miyasaka Y, Ikuta Y, Tokita S et al. Laser fluence dependence of periodic grating structures formed on metal surfaces under femtosecond laser pulse irradiation. *Phys Rev B* **82**, 165417 (2010).
88. Jia TQ, Chen HX, Huang M, Zhao FL, Li XX et al. Ultraviolet-infrared femtosecond laser-induced damage in fused silica and CaF_2 crystals. *Phys Rev B* **73**, 054105 (2006).
89. Zhou K, Jia X, Xi HX, Liu JK, Feng DH et al. Periodic surface structures on Ni-Fe film induced by a single femtosecond laser pulse with diffraction rings. *Chin Opt Lett* **15**, 022201 (2017).
90. Hashida M, Miyasaka Y, Ikuta Y, Tokita S, Sakabe S. Crystal structures on a copper thin film with a surface of periodic self-organized nanostructures induced by femtosecond laser pulses. *Phys Rev B* **83**, 235413 (2011).
91. Bashir S, Rafique MS, Nathala CS, Ajami AA, Husinsky W. Femtosecond laser fluence based nanostructuring of W and Mo in ethanol. *Phys B* **513**, 48–57 (2017).
92. Sakabe S, Hashida M, Tokita S, Namba S, Okamuro K. Mechanism for self-formation of periodic grating structures on a metal surface by a femtosecond laser pulse. *Phys Rev B* **79**, 033409 (2009).
93. Winter J, Rapp S, Schmidt M, Huber HP. Ultrafast laser processing of copper: a comparative study of experimental and simulated transient optical properties. *Appl Surf Sci* **417**, 2–15 (2017).
94. Chan WL, Averback RS, Cahill DG. Nonlinear energy absorption of femtosecond laser pulses in noble metals. *Appl Phys A* **97**, 287–294 (2009).
95. Murphy RD, Torralva B, Adams DP, Yalisove SM. Laser-induced periodic surface structure formation resulting from single-pulse ultrafast irradiation of Au microstructures on a Si substrate. *Appl Phys Lett* **102**, 211101 (2013).
96. Murphy RD, Torralva B, Adams DP, Yalisove SM. Polarization dependent formation of femtosecond laser-induced periodic surface structures near stepped features. *Appl Phys Lett* **104**,

231117 (2014).

97. Yang M, Wu Q, Chen ZD, Zhang B, Tang BQ et al. Generation and erasure of femtosecond laser-induced periodic surface structures on nanoparticle-covered silicon by a single laser pulse. *Opt Lett* **39**, 343–346 (2014).
98. Das SK, Messaoudi H, Debroy A, McGlynn E, Grunwald R. Multiphoton excitation of surface plasmon-polaritons and scaling of nanoripple formation in large bandgap materials. *Opt Mater Express* **3**, 1705–1715 (2013).
99. Liu JK, Zhao H, Cheng K, Ju JQ, Feng DH et al. Ultrafast dynamics of the thin surface plasma layer and the periodic ripples formation on GaP crystal irradiated by a single femtosecond laser pulse. *Opt Express* **27**, 37859–37876 (2019).
100. Murphy RD, Torralva B, Adams DP, Yalisove SM. Pump-probe imaging of laser-induced periodic surface structures after ultrafast irradiation of Si. *Appl Phys Lett* **103**, 141104 (2013).
101. Garcia-Lechuga M, Puerto D, Fuentes-Edfuf Y, Solis J, Siegel J. Ultrafast moving-spot microscopy: birth and growth of laser-induced periodic surface structures. *ACS Photonics* **3**, 1961–1967 (2016).
102. Jiang L, Wang AD, Li B, Cui TH, Lu YF. Electrons dynamics control by shaping femtosecond laser pulses in micro/nanofabrication: modeling, method, measurement and application. *Light Sci Appl* **7**, 17134 (2018).
103. Guay JM, Lesina AC, Baxter J, Killaire G, Ramunno L et al. Topography tuning for plasmonic color enhancement via picosecond laser bursts. *Adv Opt Mater* **6**, 1800189 (2018).
104. Giannuzzi G, Gaudiuso C, Di Franco C, Scamarcio G, Lugarà PM et al. Large area laser-induced periodic surface structures on steel by bursts of femtosecond pulses with picosecond delays. *Opt Lasers Eng* **114**, 15–21 (2019).
105. Han WN, Jiang L, Li XW, Wang QS, Li H et al. Anisotropy modulations of femtosecond laser pulse induced periodic surface structures on silicon by adjusting double pulse delay. *Opt Express* **22**, 15820–15828 (2014).
106. Zhao Z, Zhao B, Lei YH, Yang JJ, Guo CL. Laser-induced regular nanostructure chains within microgrooves of Fe-based metallic glass. *Appl Surf Sci* **529**, 147156 (2020).
107. Shi XS, Jiang L, Li X, Wang SM, Yuan YP et al. Femtosecond laser-induced periodic structure adjustments based on electron dynamics control: from subwavelength ripples to double-grating structures. *Opt Lett* **38**, 3743–3746 (2013).
108. Hasegawa S, Hayasaki Y. Holographic femtosecond laser manipulation for advanced material processing. *Adv Opt Technol* **5**, 39–54 (2016).
109. Hasegawa S, Hayasaki Y, Nishida N. Holographic femtosecond laser processing with multiplexed phase fresnel lenses. *Opt Lett* **31**, 1705–1707 (2006).
110. Hasegawa S, Hayasaki Y. Holographic femtosecond laser processing with multiplexed phase fresnel lenses displayed on a liquid crystal spatial light modulator. *Opt Rev* **14**, 208–213 (2007).
111. Li BH, Jiang L, Li XW, Lin ZM, Huang LL et al. Flexible grayscale surface patterning through spatiotemporal-interference-based femtosecond laser shaping. *Adv Opt Mater* **6**, 1801021 (2018).
112. Lin YH, Shi H, Jia TQ. Distortion and light intensity correction for spatiotemporal-interference-based spatial shaping. *Laser Optoelectron Prog* **58**, 0314002 (2021).
113. Shi H, Lin YH, Jia TQ, Cao KQ, Zhang YC et al. Efficient processing of super-hydrophobic biomimetic structures on stainless steel surfaces by spatiotemporal interference of two femtosecond laser beams based on spatial light modulator. *Acta Photon Sin* **50**, 0650110 (2021).
114. Huang J, Jiang L, Li XW, Wei QS, Wang ZP et al. Cylindrically focused nonablative femtosecond laser processing of long-range uniform periodic surface structures with tunable diffraction efficiency. *Adv Opt Mater* **7**, 1900706 (2019).
115. Zou TT, Zhao B, Xin W, Wang Y, Wang B et al. High-speed femtosecond laser plasmonic lithography and reduction of graphene oxide for anisotropic photoresponse. *Light Sci Appl* **9**, 69 (2020).
116. Dostovalov A, Bronnikov K, Korolkov V, Babin S, Mitsai E et al. Hierarchical anti-reflective laser-induced periodic surface structures (LIPSSs) on amorphous Si films for sensing applications. *Nanoscale* **12**, 13431–13441 (2020).
117. Cao KQ, Chen L, Cheng K, Sun ZR, Jia TQ. Regular uniform large-area subwavelength nanogratings fabricated by the interference of two femtosecond laser beams via cylindrical lens. *Chin Opt Lett* **18**, 093201 (2020).
118. Chen L, Cao KQ, Li YL, Liu JK, Zhang SA et al. Large-area straight, regular periodic surface structures produced on fused silica by the interference of two femtosecond laser beams through cylindrical lens. *Opto-Electron Adv* **4**, 200036 (2021).
119. Allegre OJ, Jin Y, Perrie W, Ouyang J, Fearon E et al. Complete wavefront and polarization control for ultrashort-pulse laser microprocessing. *Opt Express* **21**, 21198–21207 (2013).
120. Allegre OJ, Perrie W, Edwardson SP, Dearden G, Watkins KG. Laser microprocessing of steel with radially and azimuthally polarized femtosecond vortex pulses. *J Opt* **14**, 085601 (2012).
121. Jin Y, Allegre OJ, Perrie W, Abrams K, Ouyang J et al. Dynamic modulation of spatially structured polarization fields for real-time control of ultrafast laser-material interactions. *Opt Express* **21**, 25333–25343 (2013).
122. Ouyang J, Perrie W, Allegre OJ, Heil T, Jin Y et al. Tailored optical vector fields for ultrashort-pulse laser induced complex surface plasmon structuring. *Opt Express* **23**, 12562–12572 (2015).
123. Beresna M, Gecevičius M, Kazansky PG, Gertus T. Radially polarized optical vortex converter created by femtosecond laser nanostructuring of glass. *Appl Phys Lett* **98**, 201101 (2011).
124. Anoop KK, Rubano A, Fittipaldi R, Wang X, Paparo D et al. Femtosecond laser surface structuring of silicon using optical vortex beams generated by a *q-plate*. *Appl Phys Lett* **104**, 241604 (2014).
125. Hnatovsky C, Shvedov V, Krolikowski W, Rode A. Revealing local field structure of focused ultrashort pulses. *Phys Rev Lett* **106**, 123901 (2011).
126. Lou K, Qian SX, Wang XL, Li YN, Gu B et al. Two-dimensional microstructures induced by femtosecond vector light fields on silicon. *Opt Express* **20**, 120–127 (2012).
127. Tsibidis GD, Skoulas E, Stratakis E. Ripple formation on nickel irradiated with radially polarized femtosecond beams. *Opt Lett* **40**, 5172–5175 (2015).
128. Nivas JJJ, Allahyari E, Cardano F, Rubano A, Fittipaldi R et al.

Vector vortex beams generated by q-plates as a versatile route to direct fs laser surface structuring. *Appl Surf Sci* **471**, 1028–1033 (2019).

129. Nivas JJJ, He ST, Rubano A, Vecchione A, Paparo D et al. Direct femtosecond laser surface structuring with optical vortex beams generated by a q-plate. *Sci Rep* **5**, 17929 (2015).
130. Jia TQ, Baba M, Suzuki M, Ganeev RA, Kuroda H et al. Fabrication of two-dimensional periodic nanostructures by two-beam interference of femtosecond pulses. *Opt Express* **16**, 1874–1878 (2008).
131. Jia X, Jia TQ, Ding LE, Xiong PX, Deng L et al. Complex periodic micro/nanostructures on 6*H*-SiC crystal induced by the interference of three femtosecond laser beams. *Opt Lett* **34**, 788–790 (2009).
132. Peng NN, Huo YY, Zhou K, Jia X, Pan J et al. The development of femtosecond laser-induced periodic nanostructures and their optical properties. *Acta Phys Sin* **62**, 094201 (2013).
133. Jia X, Jia TQ, Zhang SA, Sun ZR, Qiu JR et al. Manipulation of cross-linked micro/nanopatterns on ZnO by adjusting the femtosecond-laser polarizations of four-beam interference. *Appl Phys A* **114**, 1333–1338 (2014).
134. Bonse J, Höhm S, Rosenfeld A, Krüger J. Sub-100-nm laser-induced periodic surface structures upon irradiation of titanium by Ti: sapphire femtosecond laser pulses in air. *Appl Phys A* **110**, 547–551 (2013).
135. Liao Y, Cheng Y, Liu CN, Song JX, He F et al. Direct laser writing of sub-50 nm nanofluidic channels buried in glass for three-dimensional micro-nanofluidic integration. *Lab Chip* **13**, 1626–1631 (2013).
136. Liu JK, Jia TQ, Zhou K, Feng DH, Zhang SA et al. Direct writing of 150 nm gratings and squares on ZnO crystal in water by using 800 nm femtosecond laser. *Opt Express* **22**, 32361–32370 (2014).
137. Huang M, Xu ZZ. Spontaneous scaling down of femtosecond laser-induced apertures towards the 10-nanometer level: the excitation of quasistatic surface plasmons. *Laser Photonics Rev* **8**, 633–652 (2014).
138. Miyaji G, Miyazaki K. Fabrication of 50-nm period gratings on GaN in air through plasmonic near-field ablation induced by ultraviolet femtosecond laser pulses. *Opt Express* **24**, 4648–4653 (2016).
139. Li ZZ, Wang L, Fan H, Yu YH, Chen QD et al. O-FIB: far-field-induced near-field breakdown for direct nanowriting in an atmospheric environment. *Light Sci Appl* **9**, 41 (2020).
140. Dusser B, Sagan Z, Soder H, Faure N, Colombier JP et al. Controlled nanostructrures formation by ultra fast laser pulses for color marking. *Opt Express* **18**, 2913–2924 (2010).
141. Li GQ, Li JW, Yang L, Li XH, Hu YL et al. Evolution of aluminum surface irradiated by femtosecond laser pulses with different pulse overlaps. *Appl Surf Sci* **276**, 203–209 (2013).
142. Vorobyev AY, Guo CL. Spectral and polarization responses of femtosecond laser-induced periodic surface structures on metals. *J Appl Phys* **103**, 043513 (2008).
143. Gräf S, Kunz C, Undisz A, Wonneberger R, Rettenmayr M et al. Mechano-responsive colour change of laser-induced periodic surface structures. *Appl Surf Sci* **471**, 645–651 (2019).
144. Long JY, Fan PX, Zhong ML, Zhang HJ, Xie YD et al. Superhydrophobic and colorful copper surfaces fabricated by picosecond laser induced periodic nanostructures. *Appl Surf Sci* **311**, 461–467 (2014).
145. Yao JW, Zhang CY, Liu HY, Dai QF, Wu LJ et al. Selective appearance of several laser-induced periodic surface structure patterns on a metal surface using structural colors produced by femtosecond laser pulses. *Appl Surf Sci* **258**, 7625–7632 (2012).
146. Li GQ, Li JW, Hu YL, Zhang CC, Li XH et al. Femtosecond laser color marking stainless steel surface with different wavelengths. *Appl Phys A* **118**, 1189–1196 (2015).
147. Liu W, Jiang L, Han WN, Hu J, Li XW et al. Manipulation of LIPSS orientation on silicon surfaces using orthogonally polarized femtosecond laser double-pulse trains. *Opt Express* **27**, 9782–9793 (2019).
148. Huang J, Jiang L, Li XW, Wang AD, Wang Z et al. Fabrication of highly homogeneous and controllable nanogratings on silicon via chemical etching-assisted femtosecond laser modification. *Nanophotonics* **8**, 869–878 (2019).
149. Zhang CY, Yao JW, Liu HY, Dai QF, Wu LJ et al. Colorizing silicon surface with regular nanohole arrays induced by femtosecond laser pulses. *Opt Lett* **37**, 1106–1108 (2012).
150. Hwang JS, Park JE, Kim GW, Lee H, Yang MY. Fabrication of printable nanograting using solution-based laser-induced periodic surface structure process. *Appl Surf Sci* **547**, 149178 (2021).
151. Gnilitskyi I, Gruzdev V, Bulgakova NM, Mocek T, Orazi L. Mechanisms of high-regularity periodic structuring of silicon surface by sub-MHz repetition rate ultrashort laser pulses. *Appl Phys Lett* **109**, 143101 (2016).
152. Bricchi E, Kazansky PG. Extraordinary stability of anisotropic femtosecond direct-written structures embedded in silica glass. *Appl Phys Lett* **88**, 111119 (2006).
153. Lei YH, Sakakura M, Wang L, Yu YH, Wang HJ et al. High speed ultrafast laser anisotropic nanostructuring by energy deposition control via near-field enhancement. *Optica* **8**, 1365–1371 (2021).
154. Zhang JY, Gecevičius M, Beresna M, Kazansky PG. Seemingly unlimited lifetime data storage in nanostructured glass. *Phys Rev Lett* **112**, 033901 (2014).
155. Wang HJ, Lei YH, Wang L, Sakakura M, Yu YH et al. 100-layer error-free 5D optical data storage by ultrafast laser nanostructuring in glass. *Laser Photonics Rev* **16**, 2100563 (2022).
156. Beresna M, Gecevičius M, Kazansky PG. Polarization sensitive elements fabricated by femtosecond laser nanostructuring of glass [Invited]. *Opt Mater Express* **1**, 783–795 (2011).
157. Drevinskas R, Kazansky PG. High-performance geometric phase elements in silica glass. *APL Photonics* **2**, 066104 (2017).
158. Brasselet E, Royon A, Canioni L. Dense arrays of microscopic optical vortex generators from femtosecond direct laser writing of radial birefringence in glass. *Appl Phys Lett* **100**, 181901 (2012).
159. Fernandes LA, Grenier JR, Herman PR, Aitchison JS, Marques PVS. Femtosecond laser fabrication of birefringent directional couplers as polarization beam splitters in fused silica. *Opt Express* **19**, 11992–11999 (2011).
160. Beresna M, Kazansky PG. Polarization diffraction grating produced by femtosecond laser nanostructuring in glass. *Opt Lett*

35, 1662–1664 (2010).
161. Drevinskas R, Beresna M, Gecevičius M, Khenkin M, Kazanskii AG et al. Giant birefringence and dichroism induced by ultrafast laser pulses in hydrogenated amorphous silicon. *Appl Phys Lett* **106**, 171106 (2015).
162. Drevinskas R, Beresna M, Zhang JY, Kazanskii AG, Kazansky PG. Ultrafast laser-induced metasurfaces for geometric phase manipulation. *Adv Opt Mater* **5**, 1600575 (2017).
163. Song J, Dai Y, Tao WJ, Gong M, Ma GH et al. Surface birefringence of self-assembly periodic nanostructures induced on 6H-SiC surface by femtosecond laser. *Appl Surf Sci* **363**, 664–669 (2016).
164. Cerkauskaite A, Drevinskas R, Solodar A, Abdulhalim I, Kazansky PG. Form-birefringence in ITO thin films engineered by ultrafast laser nanostructuring. *ACS Photonics* **4**, 2944–2951 (2017).
165. Zhang FZ, Chen L, Zhang YC, Jiang QL, Feng DH et al. High-performance birefringence of periodic nanostructures in FTO thin film fabricated by IR-UV femtosecond laser. *Front Phys* **10**, 861389 (2022).
166. Chen L, Cao KQ, Liu JK, Jia TQ, Li YY et al. Surface birefringence of regular periodic surface structures produced on glass coated with an indium tin oxide film using a low-fluence femtosecond laser through a cylindrical lens. *Opt Express* **28**, 30094–30106 (2020).
167. Li H, Zhang CY, Li XF, Xiang J, Tie SL et al. Enhanced upconversion luminescence from ZnO/Zn hybrid nanostructures induced on a Zn foil by femtosecond laser ablation. *Opt Express* **23**, 30118–30126 (2015).
168. Vorobyev AY, Guo CL. Femtosecond laser blackening of platinum. *J Appl Phys* **104**, 053516 (2008).
169. Vorobyev AY, Guo CL. Effects of nanostructure-covered femtosecond laser-induced periodic surface structures on optical absorptance of metals. *Appl Phys A* **86**, 321–324 (2007).
170. Vorobyev AY, Topkov AN, Gurin OV, Svich VA, Guo CL. Enhanced absorption of metals over ultrabroad electromagnetic spectrum. *Appl Phys Lett* **95**, 121106 (2009).
171. Vorobyev AY, Guo CL. Direct creation of black silicon using femtosecond laser pulses. *Appl Surf Sci* **257**, 7291–7294 (2011).
172. Yang J, Luo FF, Kao TS, Li X, Ho GW et al. Design and fabrication of broadband ultralow reflectivity black Si surfaces by laser micro/nanoprocessing. *Light Sci Appl* **3**, e185 (2014).
173. Wang PQ, Liu Z, Xu KC, Blackwood DJ, Hong MH et al. Periodic upright nanopyramids for light management applications in ultrathin crystalline silicon solar cells. *IEEE J Photovolt* **7**, 493–501 (2017).
174. Zhao QZ, Ciobanu F, Malzer S, Wang LJ. Enhancement of optical absorption and photocurrent of 6H-SiC by laser surface nanostructuring. *Appl Phys Lett* **91**, 121107 (2007).
175. Pan J, Jia TQ, Huo YY, Jia X, Feng DH et al. Great enhancement of near band-edge emission of ZnSe two-dimensional complex nanostructures fabricated by the interference of three femtosecond laser beams. *J Appl Phys* **114**, 093102 (2013).
176. Jia X, Jia TQ, Zhang Y, Xiong PX, Feng DH et al. Optical absorption of two dimensional periodic microstructures on ZnO crystal fabricated by the interference of two femtosecond laser beams. *Opt Express* **18**, 14401–14408 (2010).
177. Liu P, Wang WJ, Pan AF, Xiang Y, Wang DP. Periodic surface structures on the surface of indium tin oxide film obtained using picosecond laser. *Opt Laser Technol* **106**, 259–264 (2018).
178. Cubero Á, Martinez E, Angurel LA, De La Fuente GF, Navarro R et al. Surface superconductivity changes of niobium sheets by femtosecond laser-induced periodic nanostructures. *Nanomaterials* **10**, 2525 (2020).
179. Cubero A, Martínez E, Angurel LA, De La Fuente GF, Navarro R et al. Effects of laser-induced periodic surface structures on the superconducting properties of Niobium. *Appl Surf Sci* **508**, 145140 (2020).
180. Zuo P, Jiang L, Li X, Tian MY, Xu CY et al. Maskless micro/nanopatterning and bipolar electrical rectification of MoS_2 flakes through femtosecond laser direct writing. *ACS Appl Mater Interfaces* **11**, 39334–39341 (2019).
181. Nivas JJJ, Valadan M, Salvatore M, Fittipaldi R, Himmerlich M et al. Secondary electron yield reduction by femtosecond pulse laser-induced periodic surface structuring. *Surf Interfaces* **25**, 101179 (2021).
182. Zorba V, Stratakis E, Barberoglou M, Spanakis E, Tzanetakis P et al. Biomimetic artificial surfaces quantitatively reproduce the water repellency of a lotus leaf. *Adv Mater* **20**, 4049–4054 (2008).
183. Parker AR, Lawrence CR. Water capture by a desert beetle. *Nature* **414**, 33–34 (2001).
184. Chen F, Zhang DS, Yang Q, Yong JL, Du GQ et al. Bioinspired wetting surface via laser microfabrication. *ACS Appl Mater Interfaces* **5**, 6777–6792 (2013).
185. Yong JL, Yang Q, Chen F, Zhang DS, Farooq U et al. A simple way to achieve superhydrophobicity, controllable water adhesion, anisotropic sliding, and anisotropic wetting based on femtosecond-laser-induced line-patterned surfaces. *J Mater Chem A* **2**, 5499–5507 (2014).
186. Zouaghi S, Six T, Bellayer S, Moradi S, Hatzikiriakos SG et al. Antifouling biomimetic liquid-infused stainless steel: application to dairy industrial processing. *ACS Appl Mater Interfaces* **9**, 26565–26573 (2017).
187. Wu D, Wang JN, Wu SZ, Chen QD, Zhao S et al. Three-level biomimetic rice-leaf surfaces with controllable anisotropic sliding. *Adv Funct Mater* **21**, 2927–2932 (2011).
188. Yong JL, Chen F, Li MJ, Yang Q, Fang Y et al. Remarkably simple achievement of superhydrophobicity, superhydrophilicity, underwater superoleophobicity, underwater superoleophilicity, underwater superaerophobicity, and underwater superaerophilicity on femtosecond laser ablated PDMS surfaces. *J Mater Chem A* **5**, 25249–25257 (2017).
189. Yong JL, Chen F, Yang Q, Fang Y, Huo JL et al. Femtosecond laser induced hierarchical ZnO superhydrophobic surfaces with switchable wettability. *Chem Commun* **51**, 9813–9816 (2015).
190. Moradi S, Kamal S, Englezos P, Hatzikiriakos SG. Femtosecond laser irradiation of metallic surfaces: effects of laser parameters on superhydrophobicity. *Nanotechnology* **24**, 415302 (2013).
191. Lin Y, Han JP, Cai MY, Liu WJ, Luo X et al. Durable and robust transparent superhydrophobic glass surfaces fabricated by a femtosecond laser with exceptional water repellency and

thermostability. *J Mater Chem A* **6**, 9049–9056 (2018).
192. Moradi S, Hadjesfandiari N, Toosi SF, Kizhakkedathu JN, Hatzikiriakos SG. Effect of extreme wettability on platelet adhesion on metallic implants: from superhydrophilicity to superhydrophobicity. *ACS Appl Mater Interfaces* **8**, 17631–17641 (2016).
193. Bonse J, Koter R, Hartelt M, Spaltmann D, Pentzien S et al. Femtosecond laser-induced periodic surface structures on steel and titanium alloy for tribological applications. *Appl Phys A* **117**, 103–110 (2014).
194. Bonse J, Koter R, Hartelt M, Spaltmann D, Pentzien S et al. Tribological performance of femtosecond laser-induced periodic surface structures on titanium and a high toughness bearing steel. *Appl Surf Sci* **336**, 21–27 (2015).
195. Wang Z, Zhao QZ, Wang CW. Reduction of friction of metals using laser-induced periodic surface nanostructures. *Micromachines* **6**, 1606–1616 (2015).
196. Bonse J, Kirner SV, Koter R, Pentzien S, Spaltmann D et al. Femtosecond laser-induced periodic surface structures on titanium nitride coatings for tribological applications. *Appl Surf Sci* **418**, 572–579 (2017).
197. Wang Z, Zhao QZ. Friction reduction of steel by laser-induced periodic surface nanostructures with atomic layer deposited TiO_2 coating. *Surf Coat Technol* **344**, 269–275 (2018).
198. Kunz C, Bonse J, Spaltmann D, Neumann C, Turchanin A et al. Tribological performance of metal-reinforced ceramic composites selectively structured with femtosecond laser-induced periodic surface structures. *Appl Surf Sci* **499**, 143917 (2020).
199. Xing YQ, Wu Z, Yang JJ, Wang XS, Liu L. LIPSS combined with ALD MoS_2 nano-coatings for enhancing surface friction and hydrophobic performances. *Surf Coat Technol* **385**, 125396 (2020).
200. Lu DL, Liu ZW. Hyperlenses and metalenses for far-field super-resolution imaging. *Nat Commun* **3**, 1205 (2012).
201. Hell SW, Sahl SJ, Bates M, Zhuang XW, Heintzmann R et al. The 2015 super-resolution microscopy roadmap. *J Phys D Appl Phys* **48**, 443001 (2015).
202. Liu YL, Chen YH, Wang F, Cai YJ, Liang CH et al. Robust far-field imaging by spatial coherence engineering. *Opto-Electron Adv* **4**, 210027 (2021).
203. Weiner AM. Ultrafast optical pulse shaping: a tutorial review. *Opt Commun* **284**, 3669–3692 (2011).
204. Drever RWP, Hall JL, Kowalski FV, Hough J, Ford GM et al. Laser phase and frequency stabilization using an optical resonator. *Appl Phys B* **31**, 97–105 (1983).

Acknowledgements

This work was supported by the National Natural Science Foundation of China (12074123, 11804227, 91950112), and the Ministry of Science and Technology of China (Grant No. 2021YFA1401100), and the Foundation of 'Manufacturing beyond limits' of Shanghai. The English text of this manuscript was edited using the OSA Language Editing Services (http://languageediting.osa.org/).

Competing interests

The authors declare no competing financial interests.